Molecular and Electronic Structures, Brönsted Basicities, and Lewis Acidities of Group VIB Transition Metal Oxide Clusters

Shenggang Li and David A. Dixon*

Chemistry Department, The University of Alabama, Shelby Hall, Box 870336, Tuscaloosa, Alabama 35487-0336

Received: February 3, 2006; In Final Form: March 3, 2006

The structures and properties of transition metal oxide (TMO) clusters of the group VIB metals, $(MO_3)_n$ (M = Cr, Mo, W; $n = 1-6$), have been studied with density functional theory (DFT) methods. Geometry optimizations and frequency calculations were carried out at the local and nonlocal DFT levels with polarized valence double-ζ quality basis sets, and final energies were calculated at nonlocal DFT levels with polarized valence triple-ζ quality basis sets at the local and nonlocal DFT geometries. Effective core potentials were used to treat the transition metal atoms. Two types of clusters were investigated, the ring and the chain, with the ring being lower in energy. Large ring structures ($n > 3$) were shown to be fluxional in their out of plane deformations. Long chain structures ($n > 3$) of $(CrO_3)_n$ were predicted to be weakly bound complexes of the smaller clusters at the nonlocal DFT levels. For M_6O_{18}, two additional isomers were also studied, the cage and the inverted cage. The relative stability of the different conformations of M_6O_{18} depends on the transition metal as well as the level of theory. Normalized and differential clustering energies of the ring structures were calculated and were shown to vary with respect to the cluster size. Brönsted basicities and Lewis acidities based on a fluoride affinity scale were also calculated. The Brönsted basicities as well as the Lewis acidities depend on the size of the cluster and the site to which the proton or the fluoride anion binds. These clusters are fairly weak Brönsted bases with gas phase basicities comparable to those of H_2O and NH_3. The clusters are, however, very strong Lewis acids and many of them are stronger than strong Lewis acids such as SbF_5. Brönsted acidities of $M_6O_{19}H_2$ and $M_6O_{18}FH$ were calculated for M = Mo and W and these compounds were shown to be very strong acids in the gas phase. The acid/base properties of these TMO clusters are expected to play important roles in their catalytic activities.

Introduction

There is significant interest in the use of transition metal oxides (TMOs) as catalysts. Catalytic oxidation and acid/base chemistries account for over 90% of practical applications of metal oxides as catalysts. A fundamental understanding of TMO-catalyzed chemical transformations is needed for new catalysts to be systematically developed. For example, an important class of reactions in TMO catalysis is oxidative dehydrogenation (ODH). Alkane ODH reactions, for instance, the conversion of $CH_3CH_2CH_3$ to $CH_3CH{=}CH_2$, are not currently practiced despite extensive scientific studies[1] and their significant potential as an alternate route to alkenes,[2] because secondary combustion of primary alkene products limits yields to ~30%.[2] A model system that incorporates much of the chemistry involved in the ODH of alkanes and with a mechanism that is reasonably well established is the ODH of methanol (CH_3OH) to formaldehyde (CH_2O) where a lattice oxygen is incorporated into the water molecule.

$$CH_3OH + TMO \rightarrow CH_2O + H_2O \qquad (1)$$

In addition to the formation of CH_2O, acidic side reactions can produce CH_3OCH_3. A consideration of potential reaction mechanisms for the reactions leading to the formation of CH_2O and CH_3OCH_3 shows that fundamental properties such as the Brönsted basicity (the ability to bind a proton) and the Lewis acidity (the ability to bind an electron pair donor) of transition metal sites can play important roles in the chemistry of the TMOs. For example, addition of CH_3OH to a TMO can occur by addition of the CH_3OH to a metal site with subsequent transfer of a proton to an oxide site leaving an OCH_3 group on the metal site. Thus the balance of the Brönsted basicity of an oxygen site and the Lewis acidity of a metal site can play important roles in controlling the catalytic behavior.

Molecular clusters of TMOs have been used as models of real catalytic sites. Both experimental and computational studies have been carried out to investigate the neutral, cationic, as well as anionic clusters. Infrared spectra of CrO_3, $(MoO_3)_{1-5}$, and $(WO_3)_{1-4}$ have been measured in the gas phase[3,4] as well as in rare gas matrixes.[5−7] It is interesting to note that the structure of WO_3 in rare gas matrixes was initially suggested to be planar;[5a,6] however, the structure of MoO_3 was proposed to be pyramidal on the basis of the number of observed infrared absorption bands, suggesting that of WO_3 is pyramidal as well.[5b] The structures of $(CrO_3)_4$, $(MoO_3)_3$, and $(WO_3)_3$ were shown to be ring structures in the gas phase by electron diffraction measurements. The puckering angle was estimated to be ~39(4)° for $(CrO_3)_4$, much larger than that of ~10(5)° for $(WO_3)_3$, and $(MoO_3)_3$ was determined to have D_{3h} symmetry.[8] Mass spectroscopic measurements have been used to monitor the production of the cationic and anionic $(MO_3)_n$ (M = Cr, Mo, W; $n = 1-6$) clusters in the gas phase.[9−12] These clusters can be generated by the sublimation of the metal oxides,[10,11,12a,c,d] high power density laser ablation of the metal oxides,[9c,12e] or

10.1021/jp060735b CCC: $33.50
Published on Web 04/22/2006

low temperature and high oxygen pressure oxidation of the metals with oxygen.[12b] A number of thermodynamic properties have been measured for the molybdenum and tungsten clusters from these experiments. In addition, anion photoelectron spectroscopy has been employed by a number of groups to study these metal oxide clusters. The mononuclear, dinuclear, and trinuclear metal oxide anions, as well as the Lindqvist dianions have been studied by Wang and co-workers using this approach coupled with quantum chemical calculations.[13−18] Yoder et al. have studied the Mo_2O_{2-4} clusters,[19] and Jena and co-workers have studied the $(WO_3)_{1-4}$ clusters using a similar approach.[20] In their work, the energy for adding a WO_3 unit to the $(WO_3)_{n-1}$ cluster to form $(WO_3)_n$ is given by the differential binding energy, defined as

$$\Delta E_{\mathrm{diff},n} = -E[(MO_3)_n] + E[(MO_3)_{n-1}] + E[MO_3] \quad (2)$$

and was calculated as 4.52, 4.61, and 3.82 eV for $n = 2-4$, respectively, at the BPW91/6-311G*/Stuttgart effective core potential (SECP) level. Besides the computational studies mentioned above, there are a number of quantum chemical calculations on these metal oxide clusters reported in the literature, most of which have focused on the mononuclear and dinuclear clusters.[21] Furthermore, there is also interest in using polymetalloxalates[22] as models of catalysts. These ions can be considered to be a clathrate with an $(MO_3)_6$ cage encapsulating an anionic Brönsted base site. One of the simplest example of these polymetalloxalates is the Lindquist ion $[(MO_3)_6O]^{2-}$.

There are a number of important energetic quantities appropriate for describing the behavior of TMO catalysts including the cluster binding energies as well as the acid/base characters of the site. The gas phase Brönsted basicity is defined by the negative of the free energy of reaction 3 and the proton affinity (PA) is the negative of the enthalpy for this reaction.

$$B + H^+ \rightarrow BH^+ \quad (3)$$

If a proton is present on a neutral cluster, one can remove the proton to form an anion. The gas phase acidity is defined as the free energy of reaction 4 and the proton affinity of the anion is the enthalpy for this reaction.

$$AH \rightarrow A^- + H^+ \quad (4)$$

In addition to the interactions of protons with these clusters, it is also appropriate to consider the interaction of Lewis bases with these sites. We have recently developed a quantitative Lewis acidity scale based on calculated fluoride affinities (FAs) where the FA is defined as the negative of the enthalpy of reaction 5.[23] Due to its high basicity and small size, the fluoride

$$A + F^- \rightarrow AF^- \quad (5)$$

anion reacts with essentially all Lewis acids. This scale has enabled us to predict the Lewis acidities of a wide range of inorganic and organic molecules.

In this study, we present Brönsted basicities and Lewis acidities based on our fluoride affinity scales for the $(MO_3)_n$ ($M = Cr, Mo, W$; $n = 1-6$) clusters. In addition, we calculated the clustering energies for these species for a number of conformations. We studied structures with different numbers of μ-oxo groups to look at their effect on the binding energies and the acid/base properties. We also present the Brönsted acidities of $M_6O_{19}H_2$, $M_6O_{19}H$-, and $M_6O_{18}FH$. The calculations were done at the density functional theory (DFT) and ab initio molecular orbital theory levels.

Calculations

Extensive studies have shown that care must be taken in the calculations of the geometries and vibrational frequencies of transition metal compounds with ab initio molecular orbital methods. DFT calculations at the local and nonlocal levels usually provide good results on the geometries and frequencies for a wide range of transition metal complexes.[24] We have previously found that the local density approximation (LDA)[25] provides good geometric parameters and vibrational frequencies for transition metal compounds so we initially optimized the geometries and calculated the frequencies at this level. Geometries (minima for a given symmetry) were optimized with the Berny algorithm with redundant internal coordinates.[26] The LDA approach, however, often leads to overbinding so we have calculated the final energetics with the gradient-corrected exchange-correlation functionals B3LYP[27,28] and B88P86.[29,30] On the basis of the results of these calculations, we re-optimized the geometries of these TMO clusters at the B3LYP level. The resulting geometries at the B3LYP level are rather similar to those obtained at the LDA level except for a few cases as discussed below. To predict spectral properties of these clusers, time-dependent DFT (TD-DFT) calculations at the B3LYP level were performed to locate the lowest few singlet and triplet excited states of these metal oxide clusters. These calculations were run in the Tamm−Dancoff approximation. For the TD-DFT calculations, we used the asymptotically corrected exchange-correlation functional approach recently developed by us[31] following Casida's work[32] and based on our semiempirical ionization potential fit at the B3LYP level.[33] Entropies were calculated by using statistical mechanics approaches.[34]

We have found that a basis set of at least polarized double-ζ quality is required for reasonable calculations of geometries and frequencies at the DFT level. Basis sets at this level are available for atoms up to Xe.[35] The high atomic numbers of the second and especially the third row transition metals imply that relativistic effects must be properly accounted for to attain even semiquantitative accuracy.[36,37] For most of the properties of interest in the proposed work, the core electrons are chemically inert so one can eliminate the core contributions from direct consideration by using pseudopotentials or effective core potentials (ECPs).[38−40] We have shown that one can get excellent results for the structures and frequencies of a broad range of transition metal complexes with ECPs.[41] For this study, we have chosen the Stuttgart relativistic small core ECPs with the associated basis sets for Mo and W and polarized double-ζ DFT optimized basis sets for all other atoms for the geometry optimizations and frequency calculations. The final electronic energies were obtained with the Stuttgart basis sets[40,42] augmented by two sets of f functions and one set of g functions for the metal atoms as recommended by Martin and co-workers[43] and the aug-cc-pVTZ basis set for all other atoms. These were used for the calculations at the gradient-corrected DFT and MP2 levels. For the fluoride affinities, because we have such a large set of computational data to compare to, we calculated these values at the MP2 level with the Stuttgart ECPs and basis sets without the additional f and g functions on the transition metal atoms and the aug-cc-pVDZ basis sets on the other atoms. The fluoride affinities were calculated relative to the value of 49.9 kcal/mol obtained for CF_2O.[44] These calculations were carried out on an SGI system with the UniChem/DGauss[45] program; on the Cray XD1 and SGI Altix systems at the Alabama

TABLE 1: Relative Energies in kcal/mol for the Different Conformations of $(MO_3)_n$ (M = Cr, Mo, W; n = 3-6)

	at LDA[a] geom			at B3LYP[b] geom		
cluster	LDA[a] ΔE_{0K}	B88P86[a] ΔE_{0K}	B3LYP[c] ΔE_{0K}	B3LYP[b] ΔE_{0K}	B3LYP[c] ΔE_{0K}	B3LYP[c] $\Delta G_{298.15K}$
Cr_3O_9						
ring	0.0	0.0	0.0	0.0	0.0	0.0
chain	28.7	29.9	32.4	32.2	33.6	32.7
Cr_4O_{12}						
ring	0.0	0.0	0.0	0.0	0.0	0.0
chain	38.5	44.2	49.7	42.9	47.4	41.7
Cr_5O_{15}						
ring	0.0	0.0	0.0	0.0	0.0	0.0
chain	44.9	57.9	71.1	63.5	69.8	68.9
Cr_6O_{18}						
ring	0.0	0.0	0.0	0.0	0.0	0.0
chain	47.8	66.3	86.7	65.1	73.9	64.6
cage	−2.0	56.1	106.6	97.2	101.6	108.0
Mo_3O_9						
ring	0.0	0.0	0.0	0.0	0.0	0.0
chain	22.9	27.3	26.9	24.4	26.7	27.8
Mo_4O_{12}						
ring	0.0	0.0	0.0	0.0	0.0	0.0
chain	30.9	41.9	41.0	33.1	39.2	36.8
Mo_5O_{15}						
ring	0.0	0.0	0.0	0.0	0.0	0.0
chain	32.1	50.8	49.4	37.1	47.5	44.7
Mo_6O_{18}						
ring	0.0	0.0	0.0	0.0	0.0	0.0
cage	−65.5	3.8	14.5	5.3	14.7	25.9
chain	30.9	57.2	54.3	40.5	59.4	59.0
inverted cage	−41.1	41.5	57.8	46.0	58.9	69.5
W_3O_9						
ring	0.0	0.0	0.0	0.0	0.0	0.0
chain	24.8	29.2	26.7	23.9	25.1	25.5
W_4O_{12}						
ring	0.0	0.0	0.0	0.0	0.0	0.0
chain	30.8	41.9	34.1	28.0	33.7	30.5
W_5O_{15}						
ring	0.0	0.0	0.0	0.0	0.0	0.0
chain	29.3	48.3	36.5	27.6	34.7	33.6
W_6O_{18}						
cage	0.0	0.0	0.0	0.0	0.0	0.0
ring	102.6	32.4	33.1	36.7	26.7	15.3
inverted cage	18.0	32.4	36.7	33.5	31.3	30.6
chain	127.5	84.3	68.9	64.5	63.6	50.7

[a] DZVP2 for O and Cr, SECP for Mo and W. [b] aug-cc-pVDZ for O, SECP for Cr, Mo, and W. [c] aug-cc-pVTZ for O, SECP augmented with two sets of f functions and 1 set of g function for Cr, Mo, and W.

Supercomputer Center and a local Parallel Quantum Solutions (PQS) system with the Gaussian 03[46] program system; and on the ~2000 processor HP Linux cluster in the Molecular Science Computing Facility with the NWCHEM 4.7 program.[47] Results were visualized with the AGUI graphics system on local personal computers.[48]

Results and Discussion

Equilibrium Geometries. Relative energies are listed in Table 1 for the different conformations of the $(MO_3)_n$ clusters at the LDA and B3LYP optimized geometries. The geometries and frequencies from the LDA calculations are given as Supporting Information. The metal oxygen bond distances are listed in Table 2 for the different conformations of the $(MO_3)_n$ clusters at the B3LYP optimized geometries. Structures of these molecules are shown in Figures 1−3. The results from the B3LYP optimizations are in general consistent with the LDA calculations especially for the Mo and W clusters. For the weakly bound Cr complexes, the LDA calculations lead to substantial overbinding.

The monomer and the dimer have only one conformation. The structure of MO_3 as shown in Figure 1a is trigonal pyramidal with three equivalent metal μ-oxo bonds. For MoO_3,

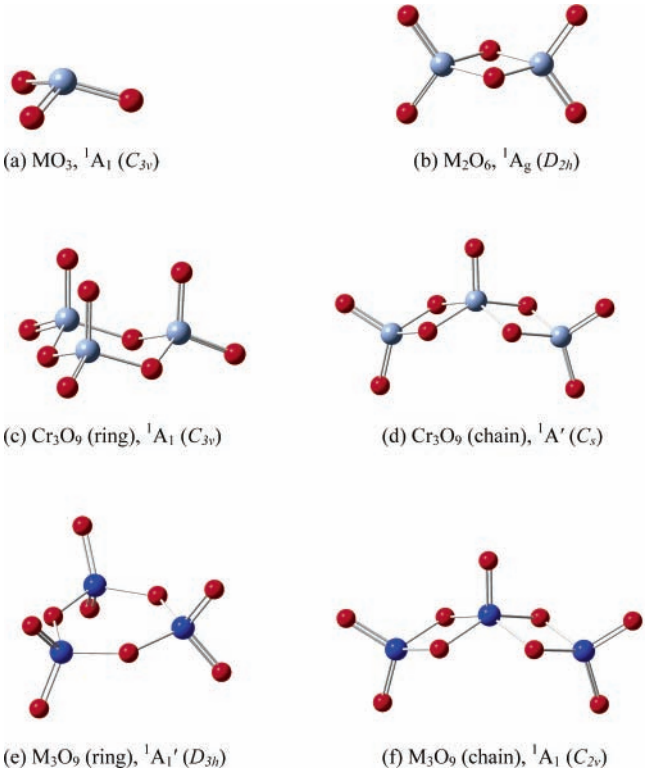

Figure 1. Equilibrium structures of $(MO_3)_n$ (M = Cr, Mo, W; n = 1−3) at the LDA level.

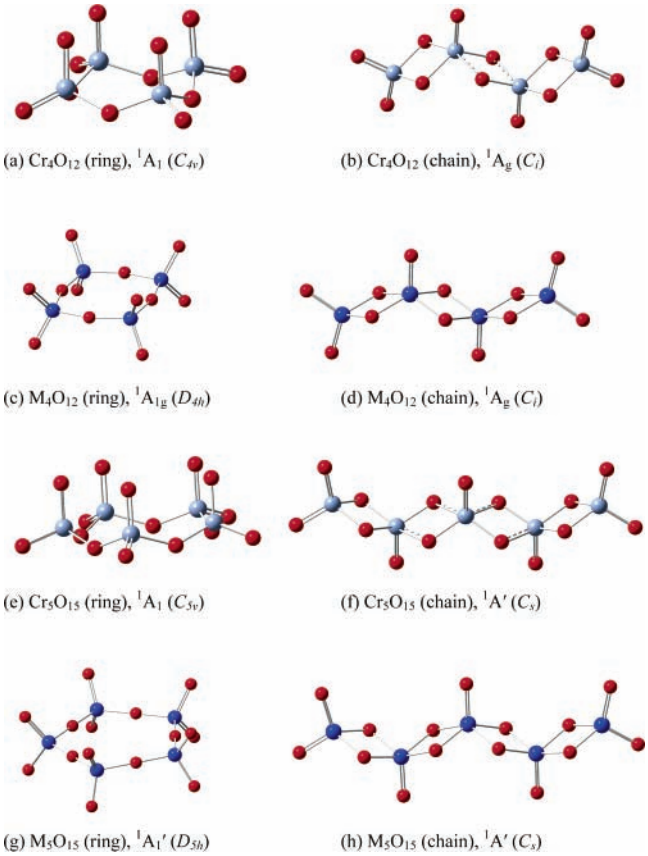

Figure 2. Equilibrium structures of $(MO_3)_n$ (M = Cr, Mo, W; n = 4, 5) at the LDA level.

this is consistent with the prediction by Weltner and co-workers on the basis of two observed absorption bands in the infrared spectrum in the rare gas matrixes.[5b] The M=O bonds are substantially elongated from Cr (1.59 Å) to Mo (1.72 Å),

TABLE 2: Metal Oxygen Bond Distances in Angstroms for $(MO_3)_n$ (M = Cr, Mo, W; $n = 1-6$) at the B3LYP/aVDZ Optimized Geometries

cluster	M=O	M−O
CrO_3	1.576 (×3)	
Cr_2O_6	1.556 (×4)	1.774 (×4)
Cr_3O_9		
ring	1.552 (×3), 1.556 (×3)	1.765 (×6)
chain	1.535, 1.559 (×4)	1.717 (×2), 1.748 (×2), 1.794 (×2), 1.895 (×2)
Cr_4O_{12}		
ring	1.553 (×8)	1.759 (×8)
chain	1.555 (×4), 1.558 (×2)	1.773 (×6), 1.775 (×2), 3.564 (×2)
Cr_5O_{15}		
ring	1.552 (×5), 1.554 (×5)	1.756 (×10)
chain	1.538 (×2), 1.550, 1.558 (×4)	1.674 (×2), 1.684 (×2), 1.728 (×2), 1.755 (×2), 1.785 (×2), 1.868 (×2), 1.904 (×2), 1.978 (×2)
Cr_6O_{18}		
ring	1.552 (×6), 1.554 (×6)	1.755 (×12)
chain	1.555 (×8), 1.558 (×4)	1.773 (×6), 1.775 (×6), 3.573 (×2), 3.690 (×2)
cage	1.537 (×6)	1.656 (×2), 1.662 (×2), 1.672 (×2), 1.678 (×2), 1.688 (×2), 1.695 (×2), 1.922 (×2), 1.940 (×2), 1.974 (×2), 1.990 (×2), 2.027 (×2), 2.058 (×2)
MoO_3	1.723 (×3)	
Mo_2O_6	1.703 (×4)	1.932 (×4)
Mo_3O_9		
ring	1.700 (×6)	1.910 (×6)
chain	1.683, 1.704 (×4)	1.915 (×4), 1.949 (×4)
Mo_4O_{12}		
ring	1.700 (×8)	1.902 (×8)
chain	1.686 (×2), 1.705 (×4)	1.843 (×2), 1.892 (×2), 1.911 (×2), 1.940 (×2), 1.992 (×2), 2.049 (×2)
Mo_5O_{15}		
ring	1.699 (×10)	1.900 (× 10)
chain	1.687 (×3), 1.705 (×4)	1.845 (×2), 1.847 (×2), 1.893 (×2), 1.914 (×2), 1.937 (×2), 1.990 (×2), 2.041 (×2), 2.046 (×2)
Mo_6O_{18}		
ring	1.699 (×12)	1.902 (×12)
chain	1.687 (×4), 1.705 (×4)	1.847 (×6), 1.893 (×2), 1.915 (×2), 1.937 (×2), 1.991 (×2), 2.038 (×2), 2.043 (×2), 2.046 (×2)
cage	1.682 (× 6)	1.929 (×24)
inverted cage	1.678, 1.682 (×4)	1.874 (×4), 1.913 (×4), 1.935 (×8), 1.938 (×4), 1.973, 2.023 (×4), 2.399 (×4), 2.618
WO_3	1.740 (×3)	
W_2O_6	1.725 (×4)	1.944 (×4)
W_3O_9		
ring	1.721 (×6)	1.919 (×6)
chain	1.704, 1.726 (×4)	1.926 (×4), 1.960 (×4)
W_4O_{12}		
ring	1.720 (×8)	1.911 (×8)
chain	1.706 (×2), 1.727 (×4)	1.925 (×4), 1.941 (×4), 1.963 (×4)
W_5O_{15}		
ring	1.720 (×10)	1.911 (×10)
chain	1.706 (×3), 1.727 (×4)	1.898 (×4), 1.914 (×2), 1.934 (×2), 1.946 (×2), 1.983 (×2), 1.986 (×2), 1.996 (×2)
W_6O_{18}		
ring	1.720 (×12)	1.912 (× 12)
chain	1.707 (×4), 1.727 (×4)	1.888 (×2), 1.896 (×2), 1.899 (×2), 1.914 (×2), 1.933 (×2), 1.948 (×2), 1.983 (×2), 1.986 (×2), 1.999 (×2), 2.006 (×2)
cage	1.705 (×6)	1.938 (×24)
inverted cage	1.701, 1.704 (×4)	1.890 (×4), 1.922 (× 4), 1.936, 1.946 (×12), 2.026 (×4), 2.425 (×4), 2.632

whereas they are slightly lengthened from Mo to W (1.74 Å). The metal oxygen bond lengths optimized at the B3LYP level agree with those obtained at the LDA level within 0.01 Å. The fact that the Mo=O bond lengths are much closer to those of W=O than Cr=O is consistent with the crystal ionic radii of the atoms at an oxidation state of VI with a coordination number of six, Cr (0.44 Å) < Mo (0.59 Å) ∼ W (0.60 Å).[49] The O=M=O bond angles decrease from Cr to Mo to W, 112°, 108°, and 105°, respectively, presumably due to the reduced repulsion among the μ-oxo groups as the metal oxygen bond lengths increase. Weltner and co-workers were able to deduce the pyramidal angle for MoO_3, which was shown to be 62(2)°, equivalent to 99° for the O=Mo=O bond angle.[5b,50] This value is smaller by about 10° as compared to our calculated O=Mo=O bond angles, 108° at the LDA level and 110° at the B3LYP level. A natural orbital population analysis[51,52] at the B3LYP level shows significant increase of positive charge on the metal atom from Cr to Mo to W, 1.33e, 1.94e, and 2.15e, respectively. We note that the ionization potentials and electronegativities increase from Cr to Mo to W (ionization potentials: 6.7665 eV for Cr, 7.09243 eV for Mo, and 7.8640 eV for W;[49] electronegativities: 1.66 for Cr, 2.16 for Mo, and 2.36 for W[53]). However, higher-order ionization potentials are much higher for Cr than for Mo and W (the second and third ionization potentials are 16.49 and 30.96 eV for Cr, and 16.16 and 27.13 eV for Mo),[49] and it is well-known that higher oxidation states of Mo and W are more stable than those of Cr.[54] The increasing ionic character from CrO_3 to MoO_3 to WO_3 is consistent with the calculated dipole moments at the B3LYP level, 3.02, 4.91, and 5.63 D, respectively. As shown in Figure

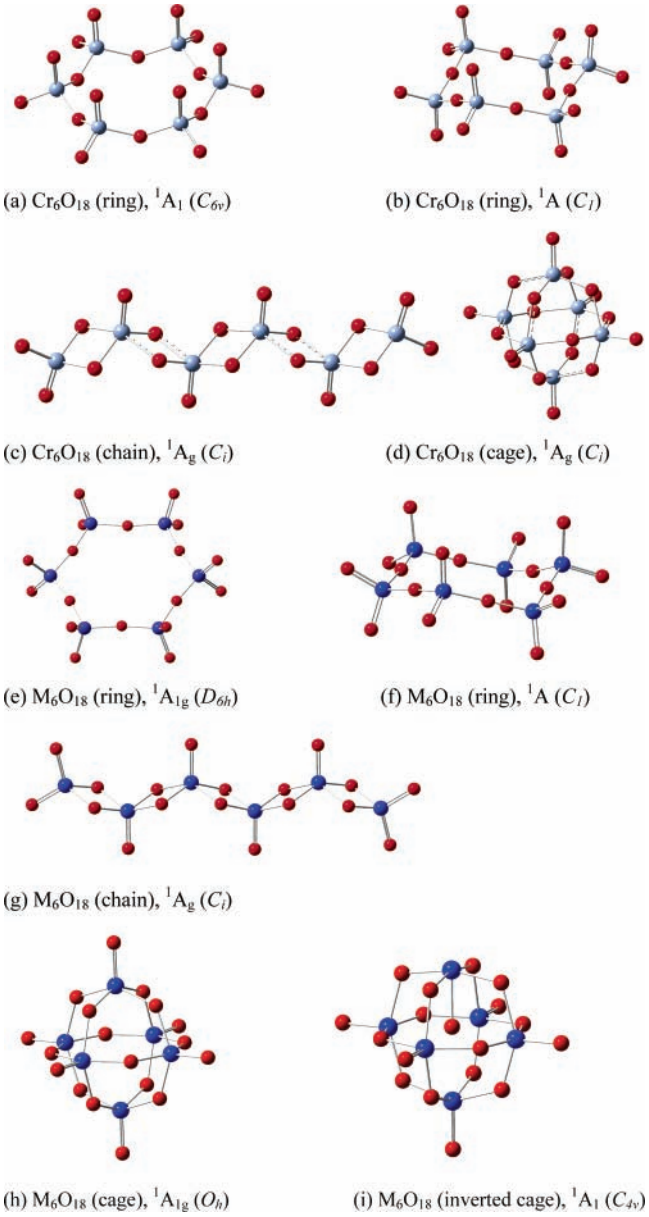

Figure 3. Equilibrium structures of M_6O_{18} (M = Cr, Mo, W) at the LDA level.

4a, the highest occupied molecular orbital (HOMO) of the monomer is predominantly of O-2pπ character.

The structure of M_2O_6 shown in Figure 1b exhibits a planar four-member ring with two bridging M−O−M bonds and two additional metal μ−oxo bonds located on each metal center. The M═O bonds are in a plane perpendicular to the plane of the ring containing the two metal and two bridging oxygen atoms. The M═O bonds in M_2O_6 are 0.01−0.02 Å shorter than those in MO_3, due to the fact that there are now two μ-oxo groups on each metal, and two M−O−M bridging interactions. The bridging M−O bonds are considerably longer than the M═O bonds. The Cr−O bonds are 0.19 Å longer than Cr═O. The difference is slightly larger for Mo and W, 0.22 and 0.21 Å, respectively. The Mo−O bonds are of similar length to the W−O bonds, both of which are considerably longer than the Cr−O bonds, similar to the case of the M═O bonds. The O═M═O bond angles, 111° for Cr_2O_6 and 110° for Mo_2O_6 and W_2O_6, are nearly identical for the three metal oxides and are comparable to those in the monomers. The O−M−O bond angles, however, are much smaller, 88° for Cr, 84° for Mo and W, due to the geometric constraint of the four-member ring

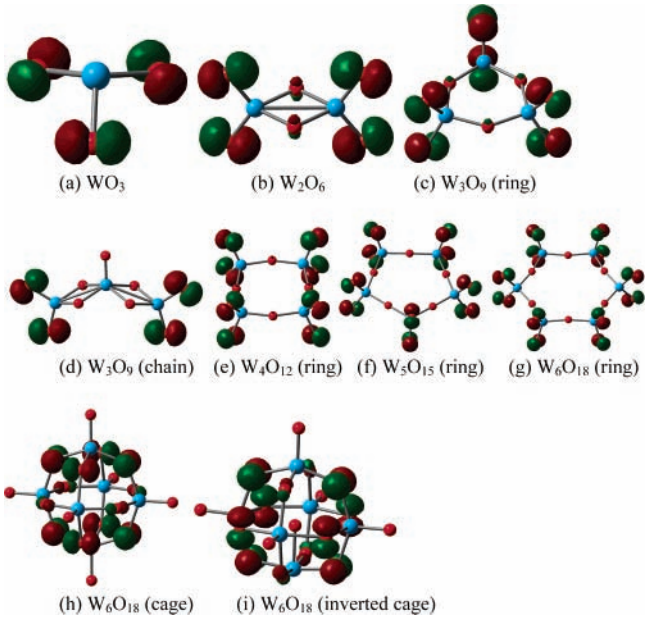

Figure 4. Highest occupied molecular orbitals of some of the $(WO_3)_n$ (n = 1−6) clusters.

structure and the much longer M−O bonds, which reduce the repulsion between the bridging oxygens. Compared to the monomer, the charge on the metal atoms in the dimer slightly decreases for Cr to 1.22e, and slightly increases for Mo and W to 2.02e and 2.33e, respectively. Furthermore, the bridge oxygens carry more negative charge than the μ-oxo oxygens. In the case of Cr_2O_6, the charge on the bridging oxygens is about twice as much as that on the μ-oxo oxygens, as shown in Table 3. This probably arises because the bridging oxygens can accept electrons from both metal atoms. The HOMO of the dimer as shown in Figure 4b is dominated by the O-2pπ orbitals on the μ-oxo oxygens.

Larger metal oxide clusters can be systematically built in two basic ways. A lower energy structure results from each metal sharing one bridge oxygen with another leading to the formation of a ring where each metal has two μ-oxo groups and two M−O−M bridge bonds. A higher energy structure is generated as a chain type structure with each terminal metal having two μ-oxo groups and each interior metal having one μ-oxo group. The metals are connected to each other by two bridging oxygens as found in the dimer. The smallest metal oxide cluster that exhibits both isomers is M_3O_9. The ring structure of M_3O_9 is a six-member ring formed by replicating the (−MO_2−O−) unit. The ring structure of Cr_3O_9 has a chair conformation as shown in Figure 1c, whereas those of Mo_3O_9 and W_3O_9 are planar as shown in Figure 1e. The planar ring structure of Cr_3O_9 is a third-order saddle point and lies about 3.4 kcal/mol higher in energy than the chair conformation at the B3LYP optimized geometries. The structure of Mo_3O_9 has been shown to be of D_{3h} symmetry by electron diffraction, consistent with our prediction.[8a] The structure of W_3O_9, however, has been estimated to have a puckering angle of about 10(5)°, although this could easily be due to the high temperature (1400° C) at which the measurement took place.[8b] Furthermore, such a small puckering angle is in reasonable agreement with our predicted planar structure. The ring structure of Cr_4O_{12}, on the other hand, has a much larger puckering angle of about 39(4)°, which is likely to be the case for Cr_3O_9 as well.[8c] The puckering angles for the Cr_3O_9 and Cr_4O_{12} ring structures are 31° and 36° at the LDA level and 27° and 34° at the B3LYP level from our calculations, in good agreement with the electron diffraction data. In addition,

TABLE 3: Charges on the Metal and Oxygen Atoms for the $(MO_3)_n$ (M = Cr, Mo, W; n = 1−6) Clusters from the Natural Orbital Population Analysis at the B3LYP/aVDZ Level

cluster	M	O═(M)	O−(M)
CrO_3	1.33	−0.44	
Cr_2O_6	1.22	−0.30	−0.61
Cr_3O_9			
ring	1.19	−0.27	−0.64
chain	1.15, 1.20(×2)	−0.14, −0.32 (×4)	−0.53 (×2), −0.55 (×2)
Cr_4O_{12} (ring)	1.20	−0.27	−0.66
Cr_5O_{15} (ring)	1.21	−0.27	−0.66
Cr_6O_{18} (ring)	1.21	−0.27	−0.67
MoO_3	1.94	−0.65	
Mo_2O_6	2.02	−0.58	−0.85
Mo_3O_9			
ring	2.03	−0.56	−0.91
chain	1.92, 2.02(×2)	−0.46, −0.59 (×4)	−0.79 (×4)
Mo_4O_{12} (ring)	2.04	−0.56	−0.93
Mo_5O_{15} (ring)	2.05	−0.56	−0.93
Mo_6O_{18}			
ring	2.05	−0.56	−0.93
cage	1.92	−0.46	−0.73
inverted cage	1.87 (×4), 1.92, 1.97	−0.41 (×4), −0.43	−0.70 (×4), −0.69 (×8), −0.95
WO_3	2.15	−0.72	
W_2O_6	2.33	−0.70	−0.94
W_3O_9			
ring	2.33	−0.67	−0.98
chain	2.26, 2.33 (×2)	−0.58, −0.70(×4)	−0.88 (×4)
W_4O_{12} (ring)	2.35	−0.67	−1.01
W_5O_{15} (ring)	2.35	−0.67	−1.01
W_6O_{18}			
ring	2.35	−0.67	−1.02
cage	2.26	−0.58	−0.84
inverted cage	2.22 (×4), 2.25, 2.33	−0.55 (×5)	−0.99, −0.82 (×4), −0.81 (×8)

the electron diffraction measurements yield bond lengths and bond angles for the W_3O_9 ring.[8c] The W═O and W−O bond lengths were measured to be 1.703(6) and 1.899(5) Å and are calculated to be 1.72 and 1.90 Å at the LDA level and 1.72 and 1.92 Å at the B3LYP level, in very good agreement with the experimental values. The O═W═O, O−W−O, and W−O−W bond angles were measured as 112(5)°, 110(3)°, and 128.0(5)°, respectively, and were calculated to be 107°, 105°, and 135° at both the LDA and B3LYP levels, in good agreement with the experimental results. Compared to the dimer, the ring trimer has comparable metal oxygen bond lengths, with the Mo−O and W−O bonds about 0.03 Å shorter. The O═M═O bond angles are also close to those in the dimer, whereas the O−M−O bond angles are much larger. This is due to the reduced geometric constraint in a six-membered ring. The charge distribution in the ring trimer is also very similar to that in the dimer, as listed in Table 3. As shown in Figure 4c, the HOMO of the ring trimer is predominantly of O-2pπ character on the μ-oxo oxygens.

The chain structures for M_3O_9 are all about 30 kcal/mol above the ring structure: 32.4 kcal/mol for Cr, 26.9 kcal/mol for Mo, and 26.7 kcal/mol for W.[55] The terminal metal centers closely resemble those in M_2O_6, whereas the interior metal center has only one M═O bond and four M−O bonds. The interior M═O bond is about 0.01−0.02 Å shorter than the terminal M═O bonds. Furthermore, not all of the M−O bonds are of equal length. The M−O bonds split into four groups for Cr_3O_9 (Figure 1d) and two groups for Mo_3O_9 and W_3O_9 (Figure 1f). The longest Cr−O bond in Cr_3O_9 is about 0.09 Å longer than that in Cr_2O_6, whereas the longest Mo−O and W−O bonds are 0.02 Å longer than those in Mo_2O_6 and W_2O_6. The Cr_3O_9 chain structure is a relatively stable structure as the binding energy for forming Cr_3O_9 from CrO_3 and Cr_2O_6 is 71.7 kcal/mol at the B3LYP level using the LDA geometries. Re-optimization at the B3LYP level led to a slight increase (<2 kcal/mol) in the binding energy to 73.2 kcal/mol. The cluster dissociation energy for M_3O_9 to MO_3 and M_2O_6 at the B3LYP level using the LDA geometries is 82.8 kcal/mol for M = Mo and 111.2 kcal/mol for M = W, respectively, somewhat higher than that for M = Cr. At the B3LYP optimized geometries, the cluster dissociation energy for M = Mo increases to 90.9 kcal/mol whereas that for M = W is essentially unchanged at 110.1 kcal/mol. The charge distributions on the metal atoms are similar to those in smaller metal oxide clusters, as shown in Table 3. The HOMO of the chain trimer is also dominated by the O-2pπ orbitals of the μ-oxo oxygens on the terminal metal centers as shown in Figure 4d.

Frameworks of larger ring structures of $(CrO_3)_n$ are nonplanar with C_{nv} symmetry as shown in Figures 2a,e and 3a, whereas those of $(MoO_3)_n$ and $(WO_3)_n$ are planar with D_{nh} symmetry as shown in Figures 2c,g and 3e. The planar ring structure is 4.6 kcal/mol for Cr_4O_{12}, 3.0 kcal/mol for Cr_5O_{15}, and 0.8 kcal/mol for Cr_6O_{18} higher in energy than the nonplanar form at the B3LYP optimized geometries. In contrast, the planar ring structure is 3.1 kcal/mol for Mo_4O_{12}, 2.8 kcal/mol for Mo_6O_{18}, 2.0 kcal/mol for W_4O_{12}, 3.4 kcal/mol for W_5O_{15}, and 7.6 kcal/mol for W_6O_{18} lower in energy than the nonplanar conformations at this level of theory. As an exception, the planar ring structure of Mo_5O_{15} was calculated to be 2.9 kcal/mol higher in energy than the nonplanar form. Thus, the heavier metal atoms are more likely to form a planar ring structure. To a good approximation, the ring conformations of M_4O_{12}, M_5O_{15}, and M_6O_{18} for Mo and W can be considered to be planar, although we note that these structures are rather fluxional in terms of moving atoms in and out of the plane and lowering the overall molecular symmetry. For example, the ring structure in a heart conformation with C_1 symmetry for Cr_6O_{18} as shown in Figure 3b is only about 0.8 kcal/mol higher in energy than that in Figure 3a. For W_6O_{18}, the chair structure with C_1 symmetry in Figure 3f is about 3.6 kcal/mol higher in energy than the one in Figure

3e. The nonplanarity of the ring structures of $(CrO_3)_n$ is likely due to the rather large repulsion between like atoms resulting from the much shorter Cr═O and Cr−O bond distances, as compared to those of Mo and W. The Mo═O and Mo−O bonds are about 0.13 and 0.14 Å longer than the Cr═O and Cr−O bonds and the W═O and W−O bonds are about 0.15 Å longer. The calculated structure of the Cr_4O_{12} ring can be compared to that obtained from the electron diffraction experiment.[8c] The Cr═O and Cr−O bond lengths were measured to be 1.580(5) and 1.775(7) Å and were calculated to be 1.57 and 1.75 Å at the LDA level and 1.55 and 1.76 Å at the B3LYP level. The experimental bond angles are 133(3)°, 97(3)°, and 128(1)° for O═Cr═O, O−Cr−O, and Cr−O−Cr, respectively, and they were calculated to be 110°, 110°, and 130° at both levels of theory. The calculated results suggest that there are substantial errors in the experimental determination of the first two angles, which deviate substantially from the predicted near tetrahedral values. There is no computational evidence for such large deviations from the tetrahedral angles as from the experimental analysis.

As the size of the ring increases, the properties of the $(MO_3)_n$ cluster exhibits a number of trends. First, the metal oxygen bond lengths, as well as their bond angles rapidly approach asymptotic values. The M═O and M−O bond distances reach the asymptotic values of 1.57 and 1.74 Å for Cr, 1.70 and 1.88 Å for Mo, and 1.72 and 1.89 Å for W at $n = 2$ for M═O and $n = 4$ for M−O. The O═M═O and O−M−O bond angles approach the tetrahedral angle as n increases. For the ring structures of $(MoO_3)_n$ and $(WO_3)_n$, the M−O−M bond angle increases as n increases until it reaches nearly 180° at $n = 5$. For $n = 6$, the M−O−M bond angles slightly bend toward the center of the ring. In the case of $(CrO_3)_n$, although the Cr−O−Cr bond angle also increases as n increases, it reaches a maximum of about 140° instead of 180° because of the nonplanarity. The calculated puckering angle for the $(CrO_3)_n$ ring cluster increases as n increases and it converges to about 35°. Second, the effective charges on the metal atoms also approach the asymptotic values of ∼1.2e for Cr, ∼2.0e for Mo, and ∼2.3e for W, as shown in Table 3. Third, as shown in Figure 4, the HOMOs of the ring structures all display O-2pπ character on the μ-oxo oxygens.

The longer chain structures are all less stable than the corresponding ring structures. The energy difference between the ring and chain structures depends on the metal. This energy difference increases as the cluster size increases and the changes are more dramatic for Cr than for Mo and W. From M_3O_9 to M_4O_{12} to M_5O_{15} to M_6O_{18}, this energy difference increases from 32.4 to 49.7 to 71.1 to 86.7 kcal/mol for Cr but only increases from 26.9 to 41.0 to 49.4 to 54.3 kcal/mol for Mo and 26.7 to 34.1 to 36.5 to 35.8 kcal/mol for W. This shows the increasing instability of the chain structure relative to the ring structure for the $(CrO_3)_n$ clusters and also shows that this energy difference for W is reasonably well converged at $n = 4$. As shown in Figures 2b,f and 3c, there are very long Cr−O bonds, marked with dashed lines, in the chain structures of Cr_4O_{12}, Cr_5O_{15}, and Cr_6O_{18}. These bonds are 0.25 Å for Cr_4O_{12}, 0.17 and 0.18 Å for Cr_5O_{15}, and 0.21 Å for Cr_6O_{18} longer than those in Cr_2O_6. Due to their low binding energies (see below) with respect to smaller cluster fragments, we re-optimized these structures at the B3LYP level. With the gradient corrected functional, the long Cr−O bonds are now 1.79 Å longer in Cr_4O_{12} and 1.80 and 1.92 Å longer in Cr_6O_{18} as compared to Cr_2O_6, substantially different from the LDA results. However, they are only 0.36 and 0.38 Å longer for Cr_5O_{15}, as compared to Cr_2O_6 in reasonable agreement with the LDA results. In comparison, the longest M−O bonds in M_4O_{12}, M_5O_{15}, and M_6O_{18} are only about 0.10 Å for Mo and 0.07 Å for W longer than those in M_2O_6. Therefore, it is appropriate to consider the Cr_4O_{12}, Cr_5O_{15}, and Cr_6O_{18} chain structures as weakly bound complexes of the smaller clusters. The fact that these are weakly bound complexes for Cr in contrast to molecules with significant interactions is consistent with LDA giving structures which are substantially overbinding. The Cr_4O_{12} chain conformation is bound with respect to two Cr_2O_6 molecules at the LDA/DZVP2 level by 18.9 kcal/mol but is unbound by 4.9 kcal/mol at the B3LYP/aVTZ//LDA/DZVP2 level. At the B3LYP/aVTZ//B3LYP/aVDZ level, the Cr_4O_{12} chain is essentially unbound with a binding energy of 0.1 kcal/mol. At this level of theory, the exothermicity to form the Cr_5O_{15} chain from one CrO_3 molecule and two Cr_2O_6 molecules is 37.9 kcal/mol. However, the Cr_5O_{15} chain is essentially unbound with respect to one Cr_2O_6 molecule and one Cr_3O_9 chain with a binding energy of −1.6 kcal/mol. Similarly, the Cr_6O_{18} chain is essentially unbound with respect to three Cr_2O_6 molecules with a binding energy of 0.4 kcal/mol. In contrast, the exothermicities for forming M_4O_{12}, M_5O_{15}, and M_6O_{18} from two M_2O_6 molecules for the tetramer, one M_2O_6 molecule and one M_3O_9 chain for the pentamer, and three M_2O_6 molecules for the hexamer are respectively 23.1, 26.8, and 50.1 kcal/mol for Mo, and 51.2, 52.6, and 104.9 kcal/mol for W at the same level of theory. The relative energies obtained at the B3LYP/aVTZ//LDA/DZVP2 level are in good agreement to those at the B3LYP/aVTZ//B3LYP/aVDZ level of theory.

We considered two additional structures for M_6O_{18}, the cage shown in Figure 3d for M = Cr and Figure 3h for M = Mo and W and the inverted cage shown in Figure 3i for M = Mo and W. The cage structure is based on the polyoxometalates (Lindquist anions) where the central Lewis base is removed to give a structure with one M═O bond and four M−O bridging bonds on each metal. For the inverted cage structure, one of the μ-oxo oxygens is inverted to point toward the center of the cage and serves as a Lewis base to stabilize the other pieces, just as in the structure of the Lindquist anion, $M_6O_{19}^{2-}$. The chemical environment around the metal atoms with metal μ-oxo bonds in the tungsten structure is similar to that in the distorted octahedral structure predicted for the c(2×2)O-terminated (100) WO_3 surface.[56] This surface structure has an octahedrally coordinated W with a W═O bond of 1.71 Å terminating the surface and the metal site trans to the W═O has a W═O bond of 1.77 Å which acts as a Lewis base with a long W−O bond distance of 2.27 Å. A similar type of distortion with smaller differences in the W−O bond distances of 1.78 Å and 2.12 Å along the c axis has been predicted[56] for the low temperature ϵ-WO_3 structure.[57] The relative stability of the different isomers of M_6O_{18} depends on the metal and on the level of theory. At the LDA level, the cage is the most stable conformation. At the B3LYP level using the LDA optimized geometries, the ring becomes the most stable one for Cr_6O_{18} and Mo_6O_{18}, whereas the cage remains the lowest energy conformation for W_6O_{18}. Re-optimization at the B3LYP level yield similar results. At the B3LYP level with the LDA geometries, the ring is 106.6 kcal/mol more stable than the cage for Cr_6O_{18}, but it is only 14.5 kcal/mol lower in energy than the cage for Mo_6O_{18}. For W_6O_{18}, the cage is 33.1 kcal/mol more stable than the ring. For Mo_6O_{18} and W_6O_{18}, the inverted cage is 43.3 and 36.7 kcal/mol respectively higher in energy than the cage. The cage structure of Cr_6O_{18} at the B3LYP optimized geometries appears to be a complex of six discrete CrO_3 molecules. Thus, it behaves in a similar way to the chain structures which also represents

TABLE 4: Normalized and Differential Clustering Energies in kcal/mol for M_2O_6 (M = Cr, Mo, W), the Ring Structures of $(MO_3)_n$ (n = 3−6), and the Cage Structure of M_6O_{18}

	normalized					differential				
	at LDA[a] geom		at B3LYP[b]geom			at LDA[a] geom		at B3LYP[b]geom		
	B88P86[a]	B3LYP[c]	B3LYP[b]	B3LYP[c]		B88P86[a]	B3LYP[c]	B3LYP[b]	B3LYP[c]	
cluster	ΔE_{0K}	ΔE_{0K}	ΔE_{0K}	ΔE_{0K}	$\Delta G_{298.15K}$	ΔE_{0K}	ΔE_{0K}	ΔE_{0K}	ΔE_{0K}	$\Delta G_{298.15K}$
Cr_2O_6	43.6	45.9	44.6	45.9	39.8	87.2	91.8	89.3	91.7	79.6
Cr_3O_9	52.7	54.5	53.3	55.0	46.6	70.9	71.7	70.7	73.2	60.2
Cr_4O_{12}	54.7	56.7	55.5	57.7	48.2	61.1	64.7	62.1	65.8	53.0
Cr_5O_{15}	55.2	57.9	55.8	58.2	48.1	57.2	62.7	57.0	60.2	47.7
Cr_6O_{18}										
ring	54.9	58.1	55.7	58.2	47.8	53.4	59.1	55.2	58.2	46.3
cage	45.6	40.3	39.5	41.3	29.8	−2.4	−47.7	−42.0	−43.2	−61.7
Mo_2O_6	47.6	55.0	53.5	54.3	47.9	95.2	110.0	106.9	108.6	95.8
Mo_3O_9	60.7	68.9	66.0	66.5	58.7	73.8	82.8	91.0	90.9	80.3
Mo_4O_{12}	64.5	72.0	68.5	69.9	60.1	75.0	82.4	76.0	80.1	64.3
Mo_5O_{15}	65.7	73.0	69.2	71.2	60.8	70.5	77.0	72.0	76.4	63.6
Mo_6O_{18}										
ring	66.0	73.2	69.5	72.6	62.4	67.5	74.2	71.0	79.6	70.4
cage	65.4	70.8	68.7	70.1	57.9	63.9	59.8	66.2	64.6	43.4
W_2O_6	50.0	60.5	58.7	59.1	52.8	100.0	121.0	117.5	118.1	105.6
W_3O_9	67.5	77.4	75.1	76.1	68.0	102.5	111.2	107.9	110.1	98.4
W_4O_{12}	72.5	81.7	78.2	80.3	70.4	85.5	94.2	87.5	92.9	77.6
W_5O_{15}	74.0	82.9	79.1	81.7	71.5	80.0	87.7	82.7	87.3	75.9
W_6O_{18}										
ring	74.5	83.2	79.5	82.7	72.4	77.0	84.7	81.5	87.7	76.9
cage	79.9	88.7	85.6	87.1	75.0	109.4	111.7	118.1	114.1	92.5

[a] DZVP2 for O and Cr, SECP for Mo and W. [b] aug-cc-pVDZ for O, SECP for Cr, Mo, and W. [c] aug-cc-pVTZ for O, SECP augmented with two sets of f functions and 1 set of g function for Cr, Mo, and W.

clusters of discrete CrO_3 or Cr_2O_6 units. The longest Cr−O bond connecting different CrO_3 units is 0.28 Å longer than the Cr−O bond in Cr_2O_6, whereas it is 0.15 Å longer at the LDA optimized geometries. This is consistent with the fact that local functionals tend to overbind, thus favoring the more compact cage structure. At the B3LYP level, although it is highly exothermic (about −240 kcal/mol) to form the Cr_6O_{18} cage from six CrO_3 molecules, it is endothermic (about 30 kcal/mol) from three Cr_2O_6 molecules. Optimized geometries at the LDA and B3LYP levels for the cage and inverted cage structures of Mo_6O_{18} and W_6O_{18} agree within 0.02 Å.

The cage structure of W_6O_{18} has O_h symmetry at both the LDA and B3LYP levels. The structure of Mo_6O_{18} at the LDA level also has O_h symmetry. At the B3LYP level, this structure has a triply degenerate imaginary frequency of ∼30i cm^{-1}, even with the ultrafine grid. Re-optimization of the Mo_6O_{18} cage structure led to a higher energy (1.2 kcal/mol) C_i symmetry structure with no imaginary frequencies. This shows that the Mo_6O_{18} cage has O_h symmetry and that the small imaginary frequencies arise from the quality of the grid. For these cage structures, the M═O bonds are about 0.01 Å shorter than those in the ring structures, whereas the M−O bonds are about 0.03 Å longer. The size of the central cavity is about 4.9 Å. For the inverted cage structure, the oxygen inside the cavity is bound to one of the metal atoms at a bond distance of about 0.07 Å for Mo and 0.03 Å for W longer than the corresponding M−O bond length in the cage structure. The five M═O bond lengths are essentially the same as those in the cage structure, whereas the M−O bond lengths on the surface of the inverted cage structure differ from those in the cage structure by as much as 0.08 Å.

The inverted cage structure of W_6O_{18} has C_{4v} symmetry at both the LDA and B3LYP levels, and that of Mo_6O_{18} has the same symmetry at the LDA level. However, at the B3LYP level the Mo_6O_{18} inverted cage of C_{4v} symmetry is again a third-order saddle point with imaginary frequencies of 103i, 103i, and 87i cm^{-1}. In this case distortion of the C_{4v} structure for the Mo_6O_{18} inverted cage led to a lower symmetry. The optimized structure of the W_6O_{18} inverted cage has five terminal W═O bond distances of 1.70 Å. The W−O bond distance to the central O (originally a W═O before inversion) lengthens to 1.94 Å and has a weak interaction with the W along the C_4 axis at a distance of 2.63 Å. This structure is qualitatively similar to the one described above for the c(2×2)O-terminated (100) WO_3 surface except that the interior oxygen has longer bond distances to the Lewis acid W and to the one it is directly bonded to because there are no crystal lattice constraints and no additional oxygen to stabilize the inverted W center with the oxygen pointing toward the center. Different from other metal oxide clusters, the HOMOs of the cage and inverted cage structures shown in Figure 4h,i are of O-2pπ characters on the bridging oxygens instead of μ-oxo oxygens.

The effects of including entropy yielding free energies (ΔG) are given in Table 1. In general the free energy differences for the different conformations are comparable to the relative energies with only zero point and electronic energy effects included. The chains are less strongly bound and have smaller frequencies. This reduces the free energy with respect to the more stable rings by up to 10 kcal/mol for the large clusters. The more compact 3-D cage structures become less stable in terms of ΔG at 298 K but the qualitative ordering of the different conformational energies does not change except for Mo_6O_{18} where the inverted cage becomes less stable than the chain at the free energy level.

Cluster Binding Energies. The normalized and differential binding energies, defined by eq 2 and

$$\Delta E_{\mathrm{norm},n} = \{-E[(MO_3)_n] + n*E[MO_3]\}/n \qquad (6)$$

are given in Table 4. The results for the ring structures for Cr show a general increase in the normalized binding energy that levels out between n = 5 and 6. The cage structure for Cr_6O_{18} clearly has a lower normalized binding energy. For the Mo and W clusters, the convergence of the normalized binding energy

TABLE 5: Vibrational Frequencies in cm^{-1} of the Metal Oxygen Stretches for $(MO_3)_n$ (M = Cr, Mo, W; $n = 1-6$) at the B3LYP/aVDZ Level

cluster	M═O	M−O
CrO_3	1075 (×2), 1012	
Cr_2O_6	1114, 1106, 1104, 1072	775, 737, 722, 478
Cr_3O_9		
ring	1114, 1104 (×2), 1100, 1078 (×2)	838 (×2), 639 (×2), 598, 570
chain	1126, 1105, 1103, 1085, 1076	846, 806, 735, 728, 674, 638, 471, 359
Cr_4O_{12} (ring)	1112, 1103, 1102 (×2), 1099, 1087 (×2), 1077	893, 875 (×2), 617, 591, 573 (×2), 541
Cr_5O_{15} (ring)	1112, 1104, 1103 (×2), 1098 (×2), 1092 (×2), 1080 (×2)	909 (×2), 873(×2), 596, 584 (×2), 541 (×2), 530
Cr_6O_{18} (ring)	1111, 1103 (×3), 1096 (×2), 1095, 1094 (×2), 1083 (×2), 1078	914, 912 (×2), 861 (×2), 595, 583, 558 (×2), 531(×3)
MoO_3	987, 961 (×2)	
Mo_2O_6	1027, 1010, 1004 (×2)	713, 696, 657, 483
Mo_3O_9		
ring	1032, 1018 (×2), 1011, 1006 (×2)	858 (×2), 658, 521 (×2), 485
chain	1046, 1014, 1009, 1005, 1004	769, 735, 695, 670, 633, 627, 465, 442
Mo_4O_{12} (ring)	1033, 1026 (×2), 1022, 1012, 1007 (×2), 1005	925, 893 (×2), 697, 448
Mo_5O_{15}(ring)	1034, 1029 (×2), 1025 (×2), 1012, 1007 (×2), 1004 (×2)	928, 927, 880 (×2), 696
Mo_6O_{18}		
ring	1035, 1030(×2), 1026(×2), 1023, 1013, 1008(×2), 1004(×2), 1003	921, 911 (×2), 856 (×2), 692
cage	1055, 1043 (×3), 1040 (×2)	849 (×2), 844 (×3), 563 (×3), 540 (×3), 531 (×3), 514 (×3)
WO_3	1001, 934 (×2)	
W_2O_6	1020, 1004, 989, 984	706, 688, 635, 501
W_3O_9		
ring	1026, 1020 (×2), 992, 987 (×2)	863 (×2), 698, 489 (×2), 480
chain	1035, 1010, 1007, 985, 983	767, 733, 705, 657, 627, 617, 484, 483
W_4O_{12} (ring)	1032, 1029 (×2), 1028, 993, 989 (×2), 987	928, 899 (×2), 744
W_5O_{15} (ring)	1035 (×2), 1030 (×2), 1029, 994, 990 (×2), 987	929 (×2), 887 (×2), 743
W_6O_{18}		
ring	1035, 1033 (×2), 1030 (×2), 1029, 995, 991 (×2), 987 (×2), 986	925, 916 (×2), 867 (×2), 739
cage	1038, 1029 (×3), 1026 (×2)	878 (×2), 861 (×3), 569 (×3), 557 (×3), 536 (×3), 532 (×3), 527, 512, 471 (×3), 447 (×2)

as a function of n for the ring structure is similar to that for Cr. The normalized binding energy for the ring clusters increases from Cr to Mo to W. The normalized binding energy for the cage cluster for $n = 6$ increases substantially from Cr to Mo to W.

The differential binding energies as calculated from eq 2 show an interesting behavior. For the ring structures of Cr, Mo, and W, the differential binding energy decreases as n increases. The most dramatic differential binding energy is found for the dimer. The differential binding energy increases from Cr to Mo to W. They are clearly not converging for Cr but do appear to be converging for Mo and W. The surprising result is that the differential binding energy for the cage structure of $n = 6$. For W, the differential binding energy for forming the cage from the ring with $n = 5$ is comparable to the energy found to form the ring with $n = 3$ from the dimer. Our differential binding energies for $n = 2-4$ for W can be compared to those of Jena and co-workers[20] who predicted values of 104.2, 106.3, and 88.1 kcal/mol, respectively. Their absolute values are smaller than ours and they find the $n = 2$ and $n = 3$ values to be comparable just as we find with the B88P86 functional. The B3LYP functional places the $n = 3$ differential binding energy well below that of the $n = 2$. From the experimentally measured enthalpies[58] for $(WO_3)_n$, $n = 2-4$, these differential binding energies are 139(24), 135(27), and 117(27) kcal/mol, respectively, in reasonable agreement with our respective calculated values, 121, 111, and 94 kcal/mol (B3LYP/aVTZ//LDA/aVDZ) and 118, 110, and 93 kcal/mol (B3LYP/aVTZ//B3LYP/aVDZ), especially considering the large experimental uncertainties.

For the normalized and differential clustering energies, the effect of including the entropy effects in terms of free energies is to reduce the energies by up to 20 kcal/mol but the qualitative observations do not change. The effect grows with increasing cluster size as expected.

Vibrational Frequencies. Harmonic vibrational frequencies of the metal oxygen stretches for the metal oxide clusters are given in Table 5 at the B3LYP level. The LDA and B3LYP frequencies are quite similar. The M═O frequencies are larger than those of M−O as expected. For MO_3, the symmetric M═O stretching frequency of the three metal oxides are all about 1000 cm^{-1}. The doubly degenerate asymmetric M═O stretch is higher than the symmetric stretch by about 80 cm^{-1} for Cr but is lower by about 30 cm^{-1} for Mo and by about 70 cm^{-1} for W. Experimentally, the symmetric stretching frequency is 890(60) cm^{-1} for CrO_3 in the gas phase[13] from a photoelectron spectroscopy measurement and the asymmetric stretching frequency was measured as 991.3 and 968.4 cm^{-1} in neon and argon matrixes, respectively.[7] Our calculated values for CrO_3 are 1002 and 1012 cm^{-1} for the symmetric stretching frequency and 1082 and 1075 cm^{-1} for the asymmetric stretching frequency at the LDA and B3LYP levels, respectively. These values are about 100 cm^{-1} larger than the experimental values. For MoO_3, the symmetric stretching frequency has been measured as 976 cm^{-1} in a neon matrix[5b] and the asymmetric stretching frequency was measured as 923.4 and 915.8 cm^{-1} in neon and argon matrixes, respectively.[7] Our calculated symmetric stretching frequencies of 992 and 987 cm^{-1} for MoO_3 at the LDA and B3LYP levels, respectively, are in excellent agreement with the experimental value as are the asymmetric stretching values of 958 and 961 cm^{-1} at the LDA and B3LYP levels. We note that the order of the symmetric and asymmetric stretching frequencies inverts between CrO_3 and MoO_3. The asymmetric stretching frequency was measured as 924.3 and 918.3 cm^{-1} for WO_3 in neon and argon matrixes, respectively,[7]

TABLE 6: Energy Gap between the Lowest Unoccupied and Highest Occupied Molecular Orbitals, ΔE(LUMO−HOMO), the Excitation Energies for the First Singlet Excited State, ΔE_S, and the First Triplet Excited State, ΔE_T, in Electronvolts at the B3LYP/aVDZ Level

cluster	ΔE(LUMO−HOMO)	ΔE_S	ΔE_T
CrO_3	3.30	1.75	1.60
Cr_2O_6	3.65	2.36	2.16
Cr_3O_9			
ring	4.20	3.03	2.62
chain	2.87	1.76	1.69
Cr_4O_{12} (ring)	4.00	2.98	2.61
Cr_5O_{15} (ring)	4.00	2.98	2.57
Cr_6O_{18} (ring)	3.64	2.76	2.45
MoO_3	3.47	2.15	2.02
Mo_2O_6	4.30	3.14	3.00
Mo_3O_9			
ring	5.08	3.97	3.55
chain	3.84	3.02	2.96
Mo_4O_{12} (ring)	4.99	4.03	3.57
Mo_5O_{15} (ring)	4.79	3.92	3.49
Mo_6O_{18}			
ring	4.56	3.83	3.45
cage	3.98	3.08	2.62
inverted cage	3.41	2.35	2.23
WO_3	3.23	1.97	1.85
W_2O_6	4.08	2.97	2.89
W_3O_9			
ring	5.51	4.29	4.01
chain	3.91	3.04	3.00
W_4O_{12} (ring)	5.39	4.40	4.03
W_5O_{15} (ring)	5.14	4.26	3.92
W_6O_{18}			
ring	4.88	4.15	3.85
cage	4.58	3.83	3.43
inverted cage	3.94	2.91	2.80

and the calculated values of 930 and 934 cm^{-1} at the LDA and B3LYP levels are in excellent agreement. This good agreement suggests that the values of 1000 and 1001 cm^{-1} for the symmetric stretch in WO_3 at the LDA and B3LYP levels are good estimates for the symmetric stretch. We note that the splitting between the symmetric and asymmetric stretch grows from Mo to W and that the symmetric stretch is of higher energy in WO_3. The agreement between the experimental and theoretical results is better for the heavier metal oxides consistent with the fact that the calculations on the Cr clusters are more difficult. For M_2O_6, four M═O and four M−O stretching frequencies can be readily identified by visualization of the normal modes. The M═O μ-oxo stretching frequencies in M_2O_6 are similar to those in MO_3, and the M−O stretching frequencies are 300−500 cm^{-1} lower. For all three dimers, the highest frequency stretches are all higher than that for the monomer and there is less spread than in the monomer. For larger clusters, the metal oxygen stretching frequencies fall into the frequency ranges exhibited by the dimer. There is little spread in the M═O frequencies and they are not strongly dependent on the structure. This suggests that although one can clearly distinguish the M═O form the M−O bonds, it will be difficult to make detailed frequency assignments for the infrared spectra of these multinuclear oxide clusters.

Excitation Energies. Table 6 lists the energy difference between the highest occupied and lowest unoccupied molecular orbitals from the B3LYP calculations, as well as the excitation energies for the first singlet and triplet excited states from the time-dependent DFT (TD-DFT) calculations. We note that the Kohn−Sham unoccupied orbitals have a different role than do the Hartree−Fock orbitals and the former are a good representation of the excited state.[31,33] For the monomer, the HOMO−LUMO energy gaps (3.2−3.5 eV) are about the same in the order MoO_3 > CrO_3 > WO_3. The actual calculated lowest excitation energies are about 1.4−1.7 eV smaller than this energy gap, because of the orbital relaxation upon electronic excitation. The lowest singlet and triplet excitation energies follow a slightly different order: CrO_3 < WO_3 < MoO_3 with the singlet states about 0.1−0.2 eV higher than the triplet states. The LUMO of MO_3 is dominated by d orbitals on the metal atom. Qualitatively, the excitation to the lowest excited state can be considered as electron transfer from the oxygen lone pair p orbitals (see Figure 4) back to the metal d orbitals.

The HOMO−LUMO energy gap, as well as the lowest excitation energy increases from the monomer to the dimer and the change is larger for Mo and W than for Cr. The LUMO of M_2O_6 is also dominated by d orbitals on the metal atoms. For the $(MO_3)_3$ ring, the LUMO is a degenerate orbital as is found for the $(MO_3)_5$ ring. For the $(WO_3)_3$ ring, there is a nondegenerate virtual orbital only 0.7 kcal/mol higher in energy than the LUMO. The LUMO for the $(MO_3)_4$ (M = Mo and W) ring is nondegenerate, but the NLUMO is degenerate with an energy difference between the LUMO and the next virtual orbital of 4.1 and 2.7 kcal/mol for M = Mo and W, respectively. This suggests that there could be very low lying states for the anions as well as suggesting that photoexcitation of the cluster could lead to different catalytic chemistries. For the ring structures, as n increases, the HOMO−LUMO energy gap, as well as the lowest excitation energy reaches its maximum at about $n = 3$ and decreases as n further increases. For M_3O_9, these energies are much lower for the chain structure than for the ring structure and those for the chain structure are fairly close to those of M_2O_6. For the different conformations of Mo_6O_{18} and W_6O_{18}, these energies follow the order ring > cage > inverted cage.

The lowest excitation energy can be considered as an approximation to the indirect band gap of a semiconductor, in our case those of MoO_3 and WO_3. To the best of our knowledge, the indirect band gap was measured to be 2.6 eV for WO_3,[59] and 3.0 eV for MoO_3.[60] Previously, Jena and co-workers have used the difference between the singlet and triplet vertical detachment energies of the anionic cluster as an approximation to the indirect band gap, and they found this energy difference increases as the size of the cluster increases and converges to the indirect band gap for W at $n = 4$.[20] As the band gap is related to the energy levels of the neutral clusters, it is more appropriate to use the lowest excitation energy of the neutral cluster as an approximation to the indirect band gap. As shown in Table 6, the lowest excitation energy for the singlet states converges to about 3.8 eV for the ring structures of $(MO_3)_n$ and 4.2 eV for those of $(WO_3)_n$. These values are substantially larger than the reported indirect band gaps. However, the lowest excitation energy for the inverted cage structure of W_6O_{18} is 2.9 eV, which is much closer to the measured indirect band gap of WO_3 of 2.6 eV. This is consistent with the fact that this cluster may serve as a model for the c(2×2)O-terminated (100) WO_3 surface and is closer to the bulk structure of WO_3. Furthermore, the indirect band gap of MoO_3 could be smaller than the measured value of 3.0 eV, as the lowest excitation energy of the inverted cage structure of Mo_6O_{18} is about 2.4 eV. Further evidence that the measured indirect band gap of MoO_3 is likely to be smaller is that the direct band gap of MoO_3 has been measured as 2.9 eV.[61] We note that a variety of band gaps have been reported in the range 2.8−3.4 eV for MoO_3 films,[62] and 2.5−3.2 eV for WO_3 films.[63]

Bronsted Basicities. The Brönsted basicities are listed in Table 7. For MO_3, the only possible site for the proton addition

TABLE 7: Brönsted Basicities in kcal/mol of $(MO_3)_n$ (M = Cr, Mo, W; n = 1−6) at the LDA Optimized Geometries

	LDA/DZVP2			B88P86/DZVP2			B3LYP/aVTZ		
	M = Cr	M = Mo	M = W	M = Cr	M = Mo	M = W	M = Cr	M = Mo	M = W
				n = 1					
	162.4	175.0	175.8	168.8	181.2	181.7	170.9	184.5	185.4
				n = 2					
=O	160.0	170.2	176.6	167.2	177.1	178.0	167.4	179.6	179.3
−O−	148.2	154.8	154.4	156.8	163.6	157.7	159.5	164.9	156.3
				n = 3					
ring									
=O	162.7	172.1	171.6	170.2	179.4	178.6	171.8	180.7	179.6
−O−	151.9	150.4	141.3	161.0	160.8	150.9	164.0	158.9	147.8
chain									
=O, center	149.8	158.2	156.8	157.1	165.2	163.3	154.2	165.9	166.6
=O, terminal	172.1	178.1	178.8	180.3	185.6	186.0	182.9	187.3	188.3
−O−	166.9	169.4	162.9	175.8	178.1	171.4	176.9	178.1	172.0
				n = 4, ring					
=O	165.3	173.1	171.9	173.3	180.3	178.9	177.3	182.7	181.3
−O−	153.5	151.1	142.9	162.9	156.6	146.4	165.6	154.8	143.4
				n = 5, ring					
=O	169.4	174.1	172.6	176.4	181.4	179.5	175.7	183.5	181.5
−O−	157.5	152.6	140.9	164.8	157.2	149.6	167.2	155.8	145.7
				n = 6					
ring									
=O		175.2	167.6		182.6	174.0		184.6	179.5
−O−		152.0	165.9		161.4	175.9		159.5	180.1
cage									
=O		167.2	172.7		173.1	179.6		178.5	181.2
−O−		172.0	141.9		181.2	150.6		186.2	146.7
inverted cage									
=O		174.5	175.4		181.6	181.3		185.2	186.2
−O−		182.4	178.2		191.4	187.1		195.0	189.7

is the oxygen as the metals are formally M(VI) centers. Thus in the formal charge sense there is a −2e charge on the O atoms. One would expect that the negatively charged O atoms would strongly attract a proton. However, the proton affinities (PAs) of the MO_3 species are not that high. For CrO_3, the PA is 171 kcal/mol, slightly higher than that of 165.1 kcal/mol at 298 K for H_2O.[64] The PA increases to ∼185 kcal/mol for MoO_3 and WO_3. The reason that these PAs are not as high as might be expected is that addition of the proton decreases the μ-oxo character in the O to which it binds, thus destabilizes this interaction.

For M_2O_6, there are two possible binding sites for the proton, the μ-oxo oxygen and the bridge oxygen. The bridge oxygen is less able to accept a proton than is the μ-oxo oxygen. In fact, the PA of the bridge oxygen is even less than that of H_2O, which is not a strong base in the gas phase. The difference in the ability of the bridge O to bind the proton as compared to that of the μ-oxo oxygen increases from Cr to Mo and W with differences of 8, 15, and 14 kcal/mol, respectively. The ability of the μ-oxo oxygen in the dimer to bind the proton is less than that of the μ-oxo oxygen in MO_3 by 4 to 6 kcal/mol.

For the larger clusters, we also have to consider proton binding to different isomers. For the ring structure of M_3O_9, the results are similar to those for the dimer with the μ-oxo oxygen having a larger PA than the bridge oxygen. There is now only one bridge oxygen between two metal atoms and its ability to bind a proton increases for M = Cr and decreases for M = Mo and W as compared to that in the dimer. The ability of the μ-oxo oxygen to bind the proton is slightly higher for M = Cr and comparable for M = Mo and W to that in the dimer. The ability of the Cr cluster to bind a proton is lower than that for the Mo or W clusters and the Mo cluster can bind a proton slightly better than the W cluster. The chain structure of M_3O_9 has a unique μ-oxo oxygen on the central metal atom, two bridging O atoms on each metal and two μ-oxo oxygens on each of the terminal metals. The single μ-oxo oxygen on the central atom is the least able to bind a proton of all of the oxygens and the terminal μ-oxo oxygens are the best site for binding the proton. The ability of the terminal μ-oxo oxygens to bind a proton is higher than those in the monomer, the dimer, or the ring trimer. The ability of the bridge oxygens to bind a proton is substantially larger than that of the dimer or the ring trimer.

Similar trends are found for larger ring clusters. For Cr, the tetramer has a larger PA for the μ-oxo oxygen as compared to the trimer as does the bridging oxygen. For Mo and W, the tetramer has a slightly larger PA for the μ-oxo oxygen but a slightly lower PA for the bridge oxygen than the trimer. For n = 5 for Cr, the PA of the bridge oxygen slightly decreases and that of the μ-oxo oxygen slightly increases as compared to the tetramer. For n = 5 and 6 for Mo and W, the PAs of both the μ=oxo and bridge oxygens increase as compared to that of the tetramer.

For n = 6, the PAs of the cage structure are quite different for Mo and W, whereas those of the ring and inverted cage are rather similar. For the Mo_6O_{18} cage, as well as the Mo_6O_{18} and W_6O_{18} inverted cages, the bridge oxygen is predicted to be protonated as compared to the μ-oxo oxygen in contrast to all of the other structures. For the W_6O_{18} cage, the PAs of the μ-oxo oxygen and bridge oxygen are predicted to be comparable. The PAs of the Mo and W cage and inverted cage compounds are among the highest for all the clusters.

The cage clusters have a site at their center that can be occupied by a Lewis base, in this case a monatomic anion. Placing an O^{2-} at the center forms the species $M_6O_{19}^{2-}$ (the Lindquist ion) and placing an F^- at the center forms the species $M_6O_{18}F^-$. These molecules can bind protons to form the neutral species $M_6O_{19}H_2$ and $M_6O_{19}FH$ as well as the anion $M_6O_{19}H^-$.

TABLE 8: Brönsted Acidities in kcal/mol of $M_6O_{19}H_2$, $M_6O_{19}H^-$ and $FM_6O_{18}H$ (M = Mo, W) at the LDA Optimized Geometries

cluster	LDA DZVP2	B88P86 DZPV2	B3LYP aVTZ
$Mo_6O_{19}H_2$	261.4	269.8	273.4
$Mo_6O_{19}H^-$	342.3	350.1	355.1
$Mo_6O_{18}FH$	258.7	268.0	258.7
$W_6O_{19}H_2$	255.3	264.5	266.7
$W_6O_{19}H^-$	335.1	343.5	347.4
$W_6O_{18}FH$	252.1	261.3	265.1

Removal of a proton from these molecules corresponds to the acidity of these species. We have previously shown that one can calculate quite reliable acidities with the approach that we are have used.[65] The acidities are given in Table 8. We predict that the acidities of $M_6O_{19}H_2$ and $M_6O_{19}FH$ to be quite low, making them very strong gas phase acids. For comparison, the acidity of H_2SO_4 is calculated to be 310.9 kcal/mol.[65] For Mo and W, we predict the acidity of $M_6O_{19}H_2$ to be 273 and 267 kcal/mol, respectively, at the B3LYP level. These values are similar to the first acidity of $PW_{12}O_{40}H_3$ of 256−258 kcal/mol depending on the site at the DFT level with the B88P86 gradient corrected functional.[66] For $M_6O_{18}FH$, we predict respective values of 259 and 265 kcal/mol for Mo and W. It is useful to note that these very acidic sites are almost overlapping with the basicities of the most basic molecules such as the imidazoles, suggesting that very basic neutral molecules could abstract a proton from these acids. The second acidities for these species (loss of a proton from $M_6O_{19}H^-$) are also quite high, 355 and 347 kcal/mol for Mo and W, respectively. These can be compared, for example, to the acidities of H_2O and H_2CO_3 which are 383.7 and 331.3 kcal/mol, respectively.[58,65] They can also be compared to the loss of a proton from $PW_{12}O_{40}H_2^-$ in the range 316−322 kcal/mol depending on the site with the B88P86 gradient corrected functional.[44]

Lewis Acidities. Table 9 lists the fluoride affinities of these species. The fluoride affinities of MO_3 are quite high, 125, 137, and 147 kcal/mol, respectively. Thus the W site is the strongest Lewis acid site. These fluoride affinities are higher than the fluoride affinities of some of the very strong Lewis acids such as SbF_5, showing the strong Lewis acid character of an MO_3 site.[23] The fluoride affinities of the dimers are substantially smaller than that of the monomer. There are two possible sites for the F^- to bind, one at the metal and one bridging between the two metals. The binding of F^- is preferred at the metal as compared to the bridging site by a substantial amount. Again, the Lewis acidity of the W dimer is the highest among the three metals. In fact the fluoride affinity of W_2O_6 is still higher than that for SbF_5. However, the FA of Cr_2O_6 is much lower, so this dimer is not a very strong Lewis acid. The fluoride affinity of the trimers is of interest because of the ring and the chain structures. For the Cr_3O_9 ring, the FA is lower than that of the dimer and it is not a very strong Lewis acid. For the Cr_3O_9 chain, the FA has substantially increased for the terminal Cr. For the Mo_3O_9 ring, the FAs for the bridging site and the terminal MO_2 site are comparable. The FA for the Mo central site in Mo_3O_9 chain is substantially less than that of the terminal site and the terminal site has an FA higher than that for the ring structure. The same holds for W_3O_9 with a substantial value of 127 kcal/mol for the terminal site in the chain structure and a value of 116 kcal/mol for the terminal MO_2 site in the ring. The FAs of the larger ring clusters are slightly higher than those of the ring trimer. For Cr, the FA of the bridge site is lower than that of the terminal MO_2 site, although their difference gets smaller as n increases. For Mo and W, the FA of the bridge site is comparable to that of the terminal MO_2 site. For $n = 6$, the FAs at the center of the cages are 135 and 145 kcal/mol, only slightly lower than those for MoO_3 and WO_3. This shows the strong Lewis acid character of the vacancy at the center of the cage. The FAs at the inverted metal centers of the inverted

TABLE 9: Fluoride Affinities (Lewis Acidities) of $(MO_3)_n$ (M = Cr, Mo, W; $n = 1-6$) at the LDA Optimized Geometries

	LDA/DZVP2			B88P86/DZVP2			B3LYP/aVTZ		
	M = Cr	M = Mo	M = W	M = Cr	M = Mo	M = W	M = Cr	M = Mo	M = W
				$n = 1$					
	120.5	128.3	136.3	121.2	129.9	138.2	124.5	137.2	147.4
				$n = 2$					
terminal	89.2	106.0	125.7	91.0	107.1	121.5	89.2	108.6	121.2
bridge		69.1	83.2		67.3	75.7		68.7	76.6
				$n = 3$					
ring									
terminal	87.4	103.0	113.0	89.2	103.9	113.7	86.9	102.4	116.2
bridge	77.9	106.5	116.3	74.8	100.2	109.6	70.1	100.6	111.7
chain									
terminal	99.2	112.6	124.8	103.9	114.4	126.3	104.2	113.1	126.8
center		94.1	103.0		94.1	102.6		91.0	103.1
				$n = 4$, ring					
terminal	92.3	106.0	115.6	92.6	106.2	116.0	89.1	106.8	118.4
bridge	94.5	119.6	129.5	87.6	109.9	120.3	82.2	106.2	118.7
				$n = 5$, ring					
terminal	96.3	107.3	116.5	95.2	107.1	116.4	91.1	108.1	119.5
bridge	101.2	118.8	129.4	94.1	110.2	120.1	87.7	109.7	122.1
				$n = 6$					
ring									
terminal		108.5	117.3		107.9	117.5		109.3	119.9
cage									
terminal		81.8	87.4		82.6	87.2		84.0	89.1
center		145.1	154.5		133.8	142.2		134.5	144.9
inverted cage									
inverted metal		156.8	170.0		155.7	169.4		161.2	175.9
M═O		76.8	81.0		79.7	81.5		79.5	82.0

cages are 161 and 176 kcal/mol for Mo and W, respectively, much higher than those for MoO_3 and WO_3. These values are some of the highest known fluoride affinities and are indicative of a site with very strong Lewis acid character. This is consistent with the stability of the polymetalloxalates and the fact that they are very strong gas phase acids. For the three different $M_6O_{18}F^-$ structures, that with the F^- at the center of the cage is the most stable for M = Mo and W. The structure with the F^- at the inverted metal center of the inverted cage is 17 and 6 kcal/mol higher in energy than the most stable structure for M = Mo and W, respectively, whereas that with the F^- at the terminal MO_2 site of the ring structure is 11 and 58 kcal/mol higher in energy.

Conclusions

The group VIB metal oxide clusters, $(MO_3)_n$ (M = Cr, Mo, W; $n = 1-6$), have been studied. Equilibrium geometries and vibrational frequencies were obtained at the local and nonlocal density functional theory (DFT) levels, whereas the energetics were calculated at gradient-corrected DFT levels, namely with the B3LYP and B88P86 functionals. Two types of conformations, the ring and the chain, were calculated, with the ring being more stable. The calculations predict very weak binding in the chain structure of $(CrO_3)_n$ ($n = 4-6$). For M_6O_{18}, two additional conformations were obtained, the cage and the inverted cage, with the cage structure being the most stable for W, slightly higher in energy than the ring structure for Mo, and the most unstable for Cr. Both normalized and differential clustering energies were calculated for the metal oxide clusters. The normalized clustering energies for the ring structures increase as the size of the cluster grows and they appear to be converging for Cr, whereas the convergence is slower for Mo and W. The differential clustering energies of the ring structures, however, decreases as the size of the cluster increases and they appear to be converging for Mo and W, but not for Cr. Both clustering energies increase from Cr to Mo to W. Calculations of the Brönsted basicites and Lewis acidities predict these clusters to be weak Brönsted bases and strong Lewis acids. Their basicities are similar to that of H_2O and the bridge oxygens are often less basic than the μ-oxo oxygens. The Lewis acidities of many of these clusters are stronger than those of strong Lewis acids such as SbF_5 and they appear to decrease as the size of the cluster increases. An exception is that the cage structure of M_6O_{18} appears to have Lewis acidities nearly identical to those of MO_3. We have also predicted clusters of the form $M_6O_{19}H_2$ and $M_6O_{18}FH$ to be very strong acids. This is due to the stability of the polymetalloxalates. The results show that these clusters can be very strong Lewis acids and so can easily accept a lone pair in a catalytic process. This is critical to the first steps in catalytic processes such as oxidative dehydrogenation of alcohols where the alcoholic oxygen can readily bond to the metal center and we will describe details of the potential energy surfaces of such processes in later publications.

Acknowledgment. We thank Dr. M. Gutowski for providing us a preprint of his paper on calculations of WO_3. This work was supported by the Chemical Sciences, Geosciences and Biosciences Division, Office of Basic Energy Sciences, U.S. Department of Energy (DOE) under grant no. DE-FG02-03ER15481 (catalysis center program). D.A.D. also thanks the Robert Ramsay Chair Fund of The University of Alabama for support. Part of this work was performed at the W. R. Wiley Environmental Molecular Sciences Laboratory, a national scientific user facility sponsored by DOE's Office of Biological and Environmental Research and located at Pacific Northwest National Laboratory, operated for the DOE by Battelle.

Supporting Information Available: Cartesian coordinates and energies for at the different levels of theory described in the text. Geometries and frequencies at the LDA level are given. Additional energy differences and relative energies are given. This material is available free of charge via the Internet at http://pubs.acs.org.

References and Notes

(1) (a) Busca, G. *Catal. Today* **1996**, *27*, 457. (b) Deo, G.; Wachs, I. E. *J. Phys. Chem.* **1991**, *95*, 5889. (c) Corma, A.; López Nieto, J. M.; Paredes, N.; Shen, Y.; Cao, H.; Suib, S. L. *Stud. Surf. Sci. Catal.* **1992**, *72*, 213. (d) Meunier, F. C.; Yasmeen, A.; Ross, J. R. H. *Catal. Today* **1997**, *37*, 33. (e) Cadus, L. E.; Gomez, M. F.; Abello, M. C. *Catal. Lett.* **1997**, *43*, 229. (f) Yoon, Y. S.; Fujikawa, N.; Ueda, W.; Moro-oka, Y.; Lee, K. W. *Catal. Today* **1995**, *24*, 327. (g) Yoon, Y. S.; Ueda, W.; Moro-oka, Y. *Top. Catal.* **1996**, *3*, 265. (h) Lee, K. H.; Yoon, Y. S.; Ueda, W.; Moro-oka, Y. *Catal. Lett.* **1997**, *46*, 267.

(2) Albonetti, S.; Cavani, F.; Trifiro, F. *Catal. Rev.-Sci. Eng.* **1996**, *38*, 413.

(3) Iorns, T. V.; Stafford, F. E. *J. Am. Chem. Soc.* **1966**, *88*, 4819.

(4) Neikirk, D. L.; Fagerli, J. C.; Smith, M. L.; Mosman, D.; Devore, T. C. *J. Mol. Spectrosc.* **1991**, *244*, 165.

(5) (a) Weltner, W., Jr.; McLeod, D., Jr. *J. Mol. Spectrosc.* **1965**, *17*, 276 and references therein. (b) Hewett, W. D., Jr.; Newton, J. H.; Weltner, W., Jr. *J. Phys. Chem.* **1975**, *79*, 2640.

(6) Green, D. W.; Ervin, K. M. *J. Mol. Spectrosc.* **1981**, *89*, 145.

(7) (a) Chertihin, G. V.; Bare, W. D.; Andrews, L. *J. Chem. Phys.* **1997**, *107*, 2798. (b) Bare, W. D.; Souter, P. F.; Andrews, L. *J. Phys. Chem. A* **1998**, *102*, 8279. (c) Zhou, M.; Andrews, L. *J. Chem. Phys.* **1999**, *111*, 4230.

(8) (a) Zasorin, E. Z.; Rambidi, N. G.; Akishin, P. A. *Acta Crystallogr., Sect. A* **1963**, *16*, 130. (b) Hargittai, I.; Hargittai, M.; Spiridonov, V. P.; Erokhin, E. V. *J. Mol. Struct.* **1971**, *8*, 31. (c) Ivanov, A. A.; Demidov, A. V.; Popenko, N. I.; Zasorin, E. Z.; Spiridonov, V. P. *J. Mol. Struct.* **1980**, *63*, 121. The puckering angle for the ring structure of $(MO_3)_n$ ($n > 2$) is defined as the dihedral angle between the O−M−O plane and the plane containing all the bridging oxygens.

(9) (a) Hachimi, A.; Poitevin, E.; Krier, G.; Muller, J. F.; Ruiz-Lopez, M. F. *Int. J. Mass Spectrosc. Ion Proc.* **1995**, *144*, 23. (b) Wang, X.; Neukermans, S.; Vanhoutte, F.; Janssens, E.; Verschoren, G.; Silverans, R. E.; Lievens, P. *Appl. Phys. B* **2001**, *73*, 417. (c) Bergeron, D. E.; Castleman, A. W. Jr.; Jones, N. O.; Khanna, S. N. *Nano Lett.* **2004**, *4*, 261.

(10) (a) Berkowitz, J.; Inghram, M. G.; Chupka, W. A. *J. Chem. Phys.* **1957**, *26*, 842. (b) Burns, R. P.; DeMaria, G.; Drowart, J.; Grimley, R. T. *J. Chem. Phys.* **1960**, *32*, 1363. (c) Fialko, E. F.; Kikhtenko, A. V.; Goncharov, V. B.; Zamaraev, K. I. *J. Phys. Chem. A* **1997**, *101*, 8607.

(11) (a) Berkowitz, J.; Chupka, W. A.; Inghram, M. G. *J. Chem. Phys.* **1957**, *27*, 85. (b) Ackermann, R. J.; Rauh, E. G. *J. Phys. Chem.* **1963**, *67*, 2596. (c) Bennett, S. L.; Lin, S.-S.; Gilles, P. W. *J. Phys. Chem.* **1974**, *78*, 266. (d) Azens, A.; Kitenbergs, M.; Kanders, U. *Vacuum* **1995**, *46*, 745. (e) Yang, Y. A.; Ma, Y.; Yao, J. N.; Loo, B. H. *J. Non-Cryst. Solids* **2000**, *272*, 71.

(12) (a) DeMaria, G.; Burns, R. P.; Drowart, J.; Inghram, M. G. *J. Chem. Phys.* **1960**, *32*, 1373. (b) Berkowitz-Mattuck, J. B.; Buchler, A.; Engelke, J. L.; Goldstein, S. N. *J. Chem. Phys.* **1963**, *39*, 2722. (c) Norman, J. H.; Staley, H. G. *J. Chem. Phys.* **1965**, *43*, 3804. (d) Maleknia, S.; Brodbelt, J.; Pope, K. *J. Am. Soc. Mass Spectrom.* **1991**, *2*, 212. (e) Aubriet, F.; Muller, J.-F. *J. Phys. Chem. A* **2002**, *106*, 6053.

(13) Gutsev, G. L.; Jena, P.; Zhai, H. J.; Wang, L. S. *J. Chem. Phys.* **2001**, *115*, 7935.

(14) Zhai, H. J.; Kiran, B.; Cui, L. F.; Li, X.; Dixon, D. A.; Wang, L. S. *J. Am. Chem. Soc.* **2004**, *126*, 16134.

(15) Zhai, H. J.; Huang, X.; Cui, L. F.; Li, X.; Li, J.; Wang, L. S. *J. Phys. Chem. A* **2005**, *109*, 6019.

(16) Huang, X.; Zhai, H.-J.; Kiran, B.; Wang, L.-S. *Angew. Chem., Int. Ed.* **2005**, *44*, 7251.

(17) Waters, T.; Wang, X. B.; Li S.; Kiran, B.; Dixon, D. A.; Wang, L. S. *J. Phys. Chem. A 109*, 11771.

(18) Yang, X.; Waters, T.; Wang, X. B.; O'Hair, R. A. J.; Wedd, A. G.; Li, J.; Dixon, D. A.; Wang, L. S. *J. Phys. Chem. A* **2004**, *108*, 10089.

(19) Yoder, B. L.; Maze, J. T.; Raghavachari, K.; Jarrold, C. C. *J. Chem. Phys.* **2005**, *122*, 094313.

(20) Sun, Q.; Rao, B. K.; Jena, P.; Stolcic, D.; Kim, Y. D.; Gantefor, G.; Castleman, A. W., Jr. *J. Chem. Phys.* **2004**, *121*, 9417.

(21) (a) Lau, K. C.; Kandalam, A. K.; Costales, A.; Pandey, R. *Chem. Phys. Lett.* **2004**, *393*, 112. (b) Veliah, S.; Xiang, K.-H.; Pandey, R.; Recio, J. M.; Newsam, J. M. *J. Phys. Chem. B* **1998**, *102*, 1126. (c) Oliveira, J.

A.; De Almeida, W. B.; Duarte, H. A. *Chem. Phys. Lett.* **2003**, *372*, 650. (d) Tsipis, A. C. *Phys. Chem. Chem. Phys.* **2000**, *2*, 1357. (e) Tsipis, A. C.; Tsipis, C. A. *J. Phys. Chem. A* **2000**, *104*, 859.

(22) (a) Pope, M. T. *Heteropoly and isopoly oxometalates*; Springer-Verlag: Berlin, 1983. (b) Lee, K. Y.; Misono, M. *Heteropoly compounds*; Handbook of Heterogeneous Catalysis, Vol. 1; Wiley-VCH: New York, 1997; pp 118−131. (c) Okuhara, T.; Mizuno, N.; Misono, M. *Adv. Catal.* **1996**, *41*, 113. (d) Kozhevnikov, I. V. *Catal. Rev. Sci. Eng.* **1995**, *37(2)*, 311. (e) Wang, Y.; Kim, A. Y.; Li, S.; Wang, L. Q.; Peden, C. H. F.; Bunker, B. C. Shape-Selective Solid Acid Catalysts Based on Tungstophosphoric Acid Supported on Mesoporous Silica. In *Shape Selective Catalysis-Chemicals Synthesis and Hydrocarbon Processing*; Song, S., Garcés, J. M., Sugi, Y., Eds.; American Chemical Society: Washington, DC, 2000; p 353.

(23) (a) Christe, K. O.; Dixon, D. A.; McLemore, D.; Wilson, W. W.; Sheehy, J.; Boatz, J. A. *J. Fluorine Chem.* **2000**, *101*, 151. (b) Dixon, D. A.; Christe, K. O. *Angew. Chem*. To be submitted. (c) *Chem. Eng. News* **2003**, Mar 3, 48−49.

(24) Sosa, C.; Andzelm, J.; Elkin, B. C.; Wimmer, E.; Dobbs, K. D.; Dixon, D. A. *J. Phys. Chem*. **1992**, *96*, 6630.

(25) (a) Vosko, S. H.; Wilk, L.; Nusair, M. *Can. J. Chem.* **1980**, *58*, 1200. (b) Slater, J. C. *Phys. Rev.* **1951**, *81*, 385. (We used the SVWN5 version as implemented in Gaussian 03.)

(26) Peng, C.; Ayala, P. Y.; Schlegel, H. B.; Frisch, M. J. *J. Comput. Chem*. **1996**, *17*, 49.

(27) Becke, A. D. *J. Chem. Phys.* **1993**, *98*, 5648.

(28) Lee, C.; Yang, W.; Parr, R. G. *Phys. Rev. B* **1988**, *37*, 785.

(29) Becke, A. D. *Phys. Rev. A* **1988**, *38*, 3098.

(30) Perdew, J. P. *Phys. Rev. B* **1986**, *33*, 8822.

(31) Hirata, S.; Zhan, C.-G.; Aprà, E.; Windus, T. L.; Dixon, D. A. *J. Phys. Chem. A* **2003**, *107*, 10154.

(32) Casida, M. E.; Salahub, D. R. *J. Chem. Phys.* **2000**, *113*, 8918.

(33) Zhan, C.-G.; Nichols, J. A.; Dixon, D. A. *J. Phys. Chem. A* **2003**, *107*, 4184.

(34) McQuarrie, D. A. *Statistical Mechanics*; University Science Books: Sausalito CA, 2000.

(35) Godbout, N., Salahub, D. R.; Andzelm, J.; Wimmer, E. *Can. J. Chem*. **1992**, *70*, 560.

(36) Wilson, S., ed. *Relativistic Effects in Atoms and Molecules*; Methods in Computational Chemistry, Vol. 2; Plenum Press: New York, 1988.

(37) Liu, W.; Kuchle, W.; Dolg, M. Ab Initio Pseudopotential and Density Functional Studies of Lanthanide and Actinide Systems. In *Handbook on the Physics and Chemistry of Rare Earths*; Gschneider, K. A., Jr., Eyring, L., Eds.; Elsevier: Amsterdam, 1995; Vol. 22, Chapter 170.

(38) Gropen, O. The Relativistic Effective Core Potential Method. In *Methods in Computational Chemistry. Vol. 2. Relativistic Effects in Atoms and Molecules*; Wilson, S., Ed.; Plenum Press: New York, 1988; p. 109.

(39) Küchle, W.; Dolg, M.; Stoll, H.; Preuss, H. *J. Chem. Phys.* **1994**, *100*, 7535 and references therein.

(40) Küchle, W.; Dolg, M.; Stoll, H.; Preuss, H. Pseudopotentials of the Stuttgart/Dresden Group 1998 (Revision: Tue Aug 11, 1998). See World Wide Website: http://www.theochem.uni-stuttgart.de/pseudopotentiale.

(41) (a) Christe, K. O.; Dixon, D. A.; Mack, H. G.; Oberhammer, H.; Pagelot, A.; Sanders, J. C. P.; Schrobilgen, G. J. *J. Am. Chem. Soc.* **1993**, *115*, 11279. (b) Casteel, W. J., Jr.; Dixon, D. A.; Mercier, H. P. A.; Schrobilgen, G. J. *Inorg. Chem.* **1996**, *35*, 4310. (c) Casteel, W. J., Jr.; Dixon, D. A.; LeBlond, N.; Lock, P. E.; Mercier, H. P. A.; Schrobilgen, G. J. *Inorg. Chem.* **1999**, *38*, 2340. (d) LeBlond, N.; Dixon, D. A.; Schrobilgen, G. J. *Inorg. Chem.* **2000**, *39*, 2473. (e) Gerken, M.; Dixon, D. A.; Schrobilgen, G. J. *Inorg. Chem.* **2000**, *39*, 4244. (f) Gerken, M.; Dixon, D. A.; Schrobilgen, G. J. *Inorg. Chem.* **2002**, *41*, 259.

(42) (a) Dolg, M.; Wedig, U.; Stoll, H.; Preuss, H. *J. Chem. Phys.* **1987**, *86*, 866. (b) Dolg, M. In *Modern Methods and Algorithms of Quantum Chemistry*; Grotendorst, J., Ed.; NIC Series 1; Julich Research Center: Julich, Germany, 2000. (c) Leininger, T.; Berning, A.; Nicklass, A.; Stoll, H.; Werner, H. J.; Flad, H. J. *Chem. Phys.* **1997**, *217*, 19.

(43) Martin, J. M. L.; Sundermann, A. *J. Chem. Phys.* **2001**, *114*, 3408.

(44) Krespan, C. G.; Dixon, D. A. *J. Fluor. Chem.* **1996**, *77*, 117.

(45) (a) Andzelm, J.; Wimmer, E.; Salahub, D. R. In *The Challenge of d and f Electrons: Theory and Computation*; Salahub, D. R., Zerner, M. C., Eds.; ACS Symposium Series, No. 394; American Chemical Society: Washington, DC, 1989; p 228. (b) Andzelm, J. In *Density Functional Theory in Chemistry*; Labanowski, J., Andzelm, J., Eds.; Springer-Verlag: New York, 1991; p 155. (c) Andzelm, J. W.; Wimmer, E. *J. Chem. Phys.* **1992**, *96*, 1280. (d) Komornicki, A.; Fitzgerald, G. *J. Phys. Chem*. **1993**, *98*, 1398.

(46) Frisch, M. J.; Trucks, G. W.; Schlegel, H. B.; Scuseria, G. E.; Robb, M. A.; Cheeseman, J. R.; Montgomery, J. A., Jr.; Vreven, T.; Kudin, K. N.; Burant, J. C.; Millam, J. M.; Iyengar, S. S.; Tomasi, J.; Barone, V.; Mennucci, B.; Cossi, M.; Scalmani, G.; Rega, N.; Petersson, G. A.; Nakatsuji, H.; Hada, M.; Ehara, M.; Toyota, K.; Fukuda, R.; Hasegawa, J.; Ishida, M.; Nakajima, T.; Honda, Y.; Kitao, O.; Nakai, H.; Klene, M.; Li, X.; Knox, J. E.; Hratchian, H. P.; Cross, J. B.; Bakken, V.; Adamo, C.; Jaramillo, J.; Gomperts, R.; Stratmann, R. E.; Yazyev, O.; Austin, A. J.; Cammi, R.; Pomelli, C.; Ochterski, J. W.; Ayala, P. Y.; Morokuma, K.; Voth, G. A.; Salvador, P.; Dannenberg, J. J.; Zakrzewski, V. G.; Dapprich, S.; Daniels, A. D.; Strain, M. C.; Farkas, O.; Malick, D. K.; Rabuck, A. D.; Raghavachari, K.; Foresman, J. B.; Ortiz, J. V.; Cui, Q.; Baboul, A. G.; Clifford, S.; Cioslowski, J.; Stefanov, B. B.; Liu, G.; Liashenko, A.; Piskorz, P.; Komaromi, I.; Martin, R. L.; Fox, D. J.; Keith, T.; Al-Laham, M. A.; Peng, C. Y.; Nanayakkara, A.; Challacombe, M.; Gill, P. M. W.; Johnson, B.; Chen, W.; Wong, M. W.; Gonzalez, C.; Pople, J. A. *Gaussian 03*, revision C.02; Gaussian, Inc.: Wallingford, CT, 2004.

(47) (a) Aprà, E.; Windus, T. L.; Straatsma, T. P.; Bylaska, E. J.; de Jong, W.; Hirata, S.; Valiev, M.; Hackler, M.; Pollack, L.; Kowalski, K.; Harrison, R.; Dupuis, M.; Smith, D. M. A.; Nieplocha, J.; Tipparaju V.; Krishnan, M.; Auer, A. A.; Brown, E.; Cisneros, G.; Fann, G.; Fruchtl, H.; Garza, J.; Hirao, K.; Kendall, R.; Nichols, J.; Tsemekhman, K.; Wolinski, K.; Anchell, J.; Bernholdt, D.; Borowski, P.; Clark, T.; Clerc, D.; Dachsel, H.; Deegan, M.; Dyall, K.; Elwood, D.; Glendening, E.; Gutowski, M.; Hess, A.; Jaffe, J.; Johnson, B.; Ju, J.; Kobayashi, R.; Kutteh, R.; Lin, Z.; Littlefield, R.; Long, X.; Meng, B.; Nakajima, T.; Niu, S.; Rosing, M.; Sandrone, G.; Stave, M.; Taylor, H.; Thomas, G.; van Lenthe, J.; Wong, A.; Zhang, Z. NWChem, A Computational Chemistry Package for Parallel Computers, Version 4.7; Pacific Northwest National Laboratory: Richland, WA 99352-0999, 2005. (b) Kendall, R. A.; Apra, E.; Bernholdt, D. E.; Bylaska, E. J.; Dupuis, M.; Fann, G. I.; Harrison, R. J.; Ju, J.; Nichols, J. A.; Nieplocha, J.; Straatsma, T. P.; Windus, T. L.; Wong, A. T. *Comput. Phys. Commun.* **2000**, *128*, 260.

(48) AMPAC 8, 1992−2004 Semichem, Inc., P.O. Box 1649, Shawnee, KS 66222.

(49) Lide, D. R., Ed. *CRC Handbook of Chemistry and Physics, Internet Version 2005*; CRC Press: Boca Raton, FL, 2005; <http://www.hbcpnetbase.com>.

(50) For a molecule XY_3 of C_{3v} symmetry, the pyramidal angle (β) is defined as the angle between the X−Y bond and the symmetry axis. The Y−X−Y bond angle (φ) is related to the pyramidal angle by $\cos\varphi = -{}^3/_2 \cos^2(90 - \beta) + 1$.

(51) Glendening, E. D.; Reed, A. E.; Carpenter, J. E.; Weinhold, F. NBO Version 3.1.

(52) (a) Reed, A. E.; Curtiss, L. A.; Weinhold, F. *Chem. Rev.* **1988**, *88*, 899. (b) Foster, J. P.; Weinhold, F. *J. Am. Chem. Soc.* **1980**, *102*, 7211. (c) Reed, A. E.; Weinhold, F. *J. Chem. Phys.* **1983**, *78*, 4066. (d) Reed, A. E.; Weinstock, R. B.; Weinhold, F. *J. Chem. Phys.* **1985**, *83*, 735. (e) Reed, A. E.; Weinhold, F. *J. Chem. Phys.* **1985**, *83*, 1736.

(53) Allred, A. L. *J. Inorg. Nucl. Chem.* **1961**, *17*, 215.

(54) Cotton F. A.; Wilkinson, G.; Murillo, C. A.; Bochmann, M. *Advanced Inorganic Chemistry*, 6th ed.; Wiley: New York, 1999.

(55) At the MP2/aVTZ level, the energy difference between the ring and the chain structures for Cr_3O_9 is much larger, 55.2 kcal/mol, as compared to 32.4 kcal/mol at the B3LYP/aVTZ level. However, the MP2 results for the energy difference for Mo and W of 32.4 and 28.7 kcal/mol, respectively, are in reasonable agreement with the B3LYP values of 26.9 and 26.7 kcal/mol. This is consistent with other results, which show that the correlation effects in compounds of the first row transition metals are often much harder to treat as compared to those in compounds of the second and third row transition metals.

(56) Yakovkin, I. N.; Gutowski, M. *Surf. Sci.*, submitted for publication.

(57) Woodward, P. M.; Sleight, A. W. Vogt, T. *J. Solid State Chem.* **1997**, *131*, 9.

(58) (a) Chase, M. W., Jr. NIST-JANAF Tables, 4th ed. *J. Phys. Chem. Ref. Data* **1998**, Mono. 9, Suppl. 1. (b) NIST Webbook, http://webbook.nist.gov

(59) Koffyberg, F. P.; Dwight, K.; Wold, A. *Solid State Comm.* **1979**, *30*, 433.

(60) Choopun, S.; Mangkorntong, P.; Subjareon, P.; Mangkorntong, N.; Tabata, H.; Kawai, T. *Jpn. Appl. Phys. Part 2: Lett., Express Lett.* **2004**, *43*, L91.

(61) Patil, P. S.; Patil, R. S. *Bull. Mater. Sci.* **1995**, *18*, 911.

(62) (a) Hanna, A. A.; Khilla, M. A. *Thermochim. Acta* **1983**, *65*, 311. (b) Miyata, N.; Suzuki, T.; Ohyama, R. *Thin Solid Films* **1996**, *281−282*, 218. (c) Sian, T. S.; Reddy, G. B. *Solar Energy Mater. Solar Cells* **2004**, *82*, 375.

(63) Davazoglou, D.; Leveque, G.; Donnadieu, A. *Solar Energy Mater.* **1988**, *17*, 379; Washizu, E.; Yamamoto, A.; Abe, Y.; Kawamura, M.; Sasaki, K. *Solid State Ionics* **2003**, *165*, 175.

(64) Peterson, K. A.; Xantheas, S. S.; Dixon, D. A.; Dunning, T. H., Jr. *J. Phys. Chem. A* **1998**, *102*, 2449.

(65) Alexeev, Y.; Windus, T. L.; Zhan, C. G.; Dixon, D. A. *Int. J. Quantum Chem.* **2005**, *102*, 775. erratum, **2005**, *104*, 379.

(66) Janik, M. J.; Campbell, K. A.; Bardin, B. B.; Davis, R. J.; Neurock, M. *Appl. Catal., A: General* **2003**, *256*, 51.